APPENDIX 3A

INITIAL EVALUATION OF CAPABILITY TO WITHSTAND TORNADOES

3A.1 INTRODUCTION AND CONCLUSIONS

Ginna Station is located in an area that is relatively tornado free. When the plant design criteria were approved for construction, tornado requirements were not considered necessary. Consequently, Ginna Station was not originally designed in accordance with current tornado requirements.

This appendix contains an analysis of the capability of the plant as built to withstand tornado effects. The adopted criterion is that the plant shall be maintained in a hot shutdown condition during and after tornado passage.

The structures and systems, or parts thereof, required for maintaining the plant in a hot shut-down condition have been checked against the following main tornado characteristics:

1. Tangential wind velocity of 300 mph.
2. External vacuum of 3 psi gauge.

The results of this analysis show that the reactor containment is capable of resisting the tornado loads and the buildings housing critical equipment will not collapse or suffer gross failure. Some of the areas in these buildings might be exposed to the weather because siding, windows, doors, or ventilation openings would blow outward if directly struck by a tornado with the characteristics previously reported. However, redundancy and physical separation give reasonable assurance that critical equipment located in these areas will perform their function. Controls for the critical equipment required for maintaining the plant in a hot shut-down condition are provided locally as well as in the control room.

In summary it is concluded that, although tornado requirements were not included in the design, there is reasonable assurance that public health and safety will not be endangered by a tornado passing through the plant site.

The appendix is organized in sections. Section 3A.1 includes the introduction and conclusions. Section 3A.2 gives a list of the systems required for maintaining the plant in a hot shut-down condition and the buildings in which they are housed. Section 3A.3 gives the status of the various areas of these buildings and indicates the critical components which are located in each. Section 3A.4 contains an analysis of the critical systems, the status of the components insofar as tornado effects are concerned, available redundancy and physical separation, and an overall conclusion on each system. Section 3A.5 deals in particular with the spent fuel pool (SFP) and the loss of pool water.

In drawing conclusions about a system or component vulnerability to tornadoes the following criteria have been adopted. A system or component is considered reasonably protected if:

1. The system or component is located inside a building which will not suffer damage from a tornado.
2. The system or component is located underground.
3. The system or component is located on a building floor that has one or more floors on top of it and is confined by other buildings.

4. The system or component is so designed and installed that no loss of function is anticipated even though the building in which it is housed might suffer damage or might be exposed to the weather. This might result from the fact that this system or component has a redundant system or component physically separated or protected such that failure of both systems or components from the same tornado effect is very unlikely.

The available redundancy gives reasonable assurance that time will be available for performing repairs on the redundant system or component.

3A.2 IDENTIFICATION OF CRITICAL SYSTEMS AND STRUCTURES

In order to maintain the plant in a safe hot shutdown condition, the following two functions must be performed:

1. Decay heat removal.
2. Reactivity control.

These systems are necessary in order to remove decay heat and control the core reactivity:

1. Steam relief system.
2. Auxiliary feedwater system.
3. Service water (SW) system.
4. Boration system.
5. Component cooling system.
6. Ventilation system.
7. Electrical system.
8. Instrumentation system.

The buildings which house the critical systems are

1. Auxiliary building.
2. Intermediate building.
3. Diesel-generator annex.
4. Screen house.
5. Control room.
6. Service building.
7. Cable tunnels.

3A.3 TORNADO EFFECTS ON STRUCTURES

3A.3.1GENERAL

All structures have been designed for wind loads in accordance with the requirements of the State of New York - State Building Construction Code. The wind loads tabulated in this code are based on a design wind velocity of 75 mph at a height of 30 ft above grade level. The stresses resulting from these loads were considered on the basis of a working strength design approach.

For purposes of this study the design of all critical structures has been checked on the basis of a limiting load factor approach wherein the loads utilized to determine the required limiting capacity of any structural element are computed as follows:

$C = (1.00 \pm 0.05)D + 1.0\ W_t + 1.0\ P_t$

Symbols used in this equation are identified as follows:

$C =$	required load capacity of section
$D =$	dead load of structure
$W_t =$	wind loads based upon 300 mph tangential wind velocity
$P_t =$	pressure load based upon an internal pressure 3 psi higher than the external pressure

3A.3.2REACTOR CONTAINMENT

Although tornado loads were not considered in the original design, this structure is capable of resisting the full strength tornado loads.

3A.3.3AUXILIARY BUILDING

Although tornado loads were not considered in the original design, this structure, up to and including the operating floor (elevation 271 ft 0 in.), is capable of resisting tornado loads. The siding on the superstructure would blow outward, thus relieving the pressure and wind load. Components and systems on the operating floor and above are susceptible to impact by falling debris and potential missiles. The equipment on the auxiliary building operating floor that is required to maintain the plant in a hot shutdown condition is as follows:

1. Boric acid storage tanks, pumps, and filter.
2. 480-V switchgear (bus 14).

The equipment in item 1 is surrounded by a radiological shield wall as shown in Figure 1. This wall offers significant lateral protection against potential missiles. Furthermore, the two tanks and pump are redundant. Therefore, there is reasonable assurance that there will be no loss of boration function. More details are given in Section 3A.4.2.

Damage to bus 14 will not cause loss of power supply since an independent and redundant bus (bus 16) is provided on the intermediate floor of the auxiliary building. This floor, as

previously mentioned, will not be exposed to the weather. More details are given in Section 3A.4.4.

In addition, the spent fuel pool (SFP) has been evaluated. Potential missiles may puncture the spent fuel pool (SFP) liner but will not penetrate through the concrete walls or base causing gross leakage of water.

3A.3.4INTERMEDIATE BUILDING

This structure, as shown in Figure 2, is significantly confined by other buildings, i.e., the service building, turbine building, reactor containment, and auxiliary building. Consequently, a direct exposure to a tornado funnel is extremely remote. Due to the relative vacuum which might be created by a tornado outside of the intermediate building lateral walls may blow outward. This will relieve the pressure differential and prevent gross failure of the structural steel framing, columns, and floors. Therefore, the two floors which house critical equipment, i.e., floors at elevations 253 ft 6 in. and 278 ft 4 in., are afforded significant shielding by the adjoining structures and higher floor/roof elevations.

The critical components in this structure consist of the following:

1. On floor elevation 253 ft 6 in.: two motor-driven and one turbine-driven auxiliary feedwater pumps.
2. On floor elevation 278 ft 4 in.: the cross-connection on main steam and feedwater lines to the two steam generators.

As previously mentioned, no damage is anticipated to the equipment located on these two floors. More details are given in Section 3A.4.1.

3A.3.5DIESEL-GENERATOR ANNEX

The availability of onsite diesel power was reviewed on the basis of the assumption that the tornado could cause a loss of offsite power.

Siding, windows, doors, and ventilation openings would blow outward, thus relieving the pressure loading. Damage to the roof might result if the differential pressure is not relieved in time. Two redundant diesel generators are provided. No physical damage to the diesels is anticipated. Furthermore, the physical separation between them is such that one missile would not be able to impact against both diesel generators, as shown in Figure 3. More details are given in Section 3A.4.4. The conclusion has been drawn that the emergency power supply is reasonably ensured.

3A.3.6SCREEN HOUSE

Siding, windows, doors, and ventilation openings would blow outward, thus relieving the pressure loading. No structural collapse is expected. The critical equipment housed in the screen house is represented by:

1. Four service water (SW) pumps.
2. 480-V switchgear buses 17 and 18.

The four service water (SW) pumps are redundant and sufficient physical separation exists between them to make extremely unlikely the failure of all four pumps from the same tornado effect, as shown in Figure 4.

Service water (SW) pumps 1A and 1C are energized from bus 18 and service water (SW) pumps 1B and 1D are energized from bus 17. Cross-tie between the two buses is available.

The two buses are located in the screen house and are physically separated. Therefore, there is reasonable assurance that at least one service water (SW) pump-bus combination will operate properly. More details are given in Section 3A.4.4.

3A.3.7CONTROL ROOM

No gross failure of this structure is anticipated. The only wall directly exposed is the east wall. The siding of this wall would blow outward relieving the pressure differential and leaving the interior exposed to the weather. The same would be true for windows, doors, and ventilation openings.

Local controls for the equipment required for maintaining the plant in a hot shutdown condition have been provided as a backup to the controls available in the control room. Therefore, there is reasonable assurance that controls for the critical components will be available.

3A.3.8SERVICE BUILDING

The status of this building is similar to that of the auxiliary building. The siding on the superstructure above elevation 271 ft would blow outward, thus relieving the pressure and wind loads. The components which might be affected by a tornado are the two condensate storage tanks (CST). There is reasonable assurance that the feedwater supply will be maintained because of the available redundancy and the fact that two-thirds of the tank volume is below grade.

3A.3.9CABLE TUNNELS

The cable tunnels are located underground and are capable of withstanding tornado loads.

3A.4 TORNADO EFFECTS ON THE SYSTEMS REQUIRED FOR HOT SHUTDOWN

3A.4.1DECAY HEAT REMOVAL

With the plant in a hot shutdown condition, decay heat is removed via the steam generators. In order to achieve this heat transfer, water has to be supplied to the secondary side of the steam generators and steam has to be discharged from them. For this function to be performed, it is necessary to have a source of feedwater, pumps to transfer the feedwater from the tank to the steam-generator secondary side, and steam relief from the steam generators.

3A.4.1.1Steam Relief System

Since a tornado could cause a loss of offsite power, condenser vacuum could not be maintained to allow steam discharge to the condenser. The only available route would be to the atmosphere.

On the steam pipe associated with each steam generator, outside the containment, are four steam relief valves (12.5% of full flow per valve). Figure 5 shows the location of these valves. Significant valve redundancy is available since no more than 2% full flow capacity would be needed a few seconds after shutdown.

The relief valves are located inside the intermediate building and the two sets have a minimum distance between them of 35 ft. Since the valves are relatively heavy steel, they are expected to withstand the effect of falling debris without physical damage.

The centerline of the pipe on which they are installed is at elevation 281 ft 4 in. The bulk of the steam piping is located in the intermediate building, with the exception of a run of the main steam line from steam generator B. This steel pipe being relatively thick-walled, it is also expected to withstand falling debris without sustaining serious damage.

Because of the inherent physical strength of the equipment involved, its redundancy and physical separation, it can be concluded that the steam relief function is ensured.

3A.4.1.2Auxiliary Feedwater System

This system consists of

1. One auxiliary steam-driven feedwater pump.
2. Two auxiliary motor-driven feedwater pumps.
3. Two condensate storage tanks (CST).

The steam-driven pump has the capacity of supplying water to either or both steam generators. This pump is located in the intermediate building on the northwest side at 253 ft 6 in. floor elevation. Local shielding is provided as shown in Figure 6.

The two motor-driven pumps are also located in the intermediate building on the northwest side at 253 ft 6 in. floor elevation. Each pump is sized for the water supply to one steam generator. Piping and valve arrangements allow flow to either of the two steam generators.

The distance between the shafts of the two motor-driven pumps is 8 ft, while the minimum distance between the steam-driven and the two motor-driven pumps is about 36 ft, as shown in Figure 6.

The preferred auxiliary feedwater lines from the condensate storage tank to the suction of the pumps are partly located below grade and partly inside the intermediate building. The preferred auxiliary feedwater lines from the discharge of the pumps to the steam generators are run at elevation 271 ft 0 in. before penetrating the containment.

The power supply to the motors of the two motor-driven pumps is from buses 14 and 16 located in the auxiliary building on the operating floor and on the intermediate floor, respectively.

Pump control is performed from the control room or from a local panel in the intermediate building at 253 ft 6 in. floor elevation.

The main source of water supply is by gravity feed from the condensate storage tank located in the service building on the southwest side at 253 ft 6 in. floor elevation. The feedwater suction is at 254 ft 10 in. floor elevation.

If the condensate storage tank water is not available, feedwater can be delivered to the suction of the preferred auxiliary feedwater pumps by the service water (SW) pumps. This system is described in Section 3A.4.1.3.

Because of the location of the intermediate building, the location of the required pumps, connecting piping, control and electrical cables, and redundancy and physical separation, it is concluded that the preferred auxiliary feedwater supply function is ensured.

3A.4.1.3Service Water System

This system is required for providing cooling to the emergency diesel generators and the containment ventilation system, as well as being an alternate source of preferred auxiliary feedwater. This system consists of the following components:

1. Four service water (SW) pumps.
2. Valves and piping.

Each of the four service water (SW) pumps is capable of carrying the emergency cooling load. These pumps are in the screen house, located about 115 ft north of the turbine building and about 80 ft south of the lake shore (Figure 2). The suction point from the lake water, associated piping, and valves are inside the building, below grade, in a reinforced-concrete structure. The service water (SW) piping which supplies water to the critical components is run underground from the screen house to the area being served.

Two pumps are connected to 480-V bus 18 and two to bus 17. In the event of loss of all outside power, bus 18 is energized by one diesel generator and bus 17 by the other one. Buses 17 and 18 are located inside the screen house. The electrical connections from the diesels to buses 17 and 18 are routed inside a separate underground duct bank from the diesel-generator annex building to the screen house.

Because of redundancy and physical separation, it is concluded that the function of the service water (SW) system is not jeopardized.

Additional redundancy of water supply which can be used instead of the condensate water and the service water (SW) is represented by the domestic water and the fire system.

The pumping station of the domestic water is located 2 miles away from the plant and the piping is routed underground to the plant itself. The two fire pumps, having a capacity of 2000 gpm minimum each, are located in the screen house. The time necessary for these two systems to operate is estimated to be approximately 10 minutes.

3A.4.2 REACTIVITY CONTROL

3A.4.2.1 Boration System

The reactivity control systems are required to make and hold the core subcritical following a tornado. After control rod insertion, shutdown capability is provided by boric acid injection to compensate for the long-term xenon decay transient. The system required for performing this function is the boration system.

This system is not required to operate immediately but after a period of at least 15 hr, i.e., the time required for the xenon to build up and then decay to the level present before shutdown. Therefore, ample time would be available for repair of the system.

The boration system includes the components listed below:

1. Two boric acid storage tanks.
2. Two boric acid transfer pumps.
3. One boric acid filter.
4. Three charging pumps.
5. Associated piping and cables.
6. Heat tracing.

The boric acid storage tanks, boric acid transfer pumps, and filters are located in the auxiliary building, northeast side, at elevation 271 ft. They are surrounded by a radiological shield wall, as shown in Figure 1. The siding of the auxiliary building above elevation 271 ft is not likely to withstand tornado winds or differential pressure; however, lateral protection is offered by the radiological shield wall. Furthermore, the boric acid transfer pumps and tanks have redundancy and physical separation. The three charging pumps are located on the basement floor of the auxiliary building and only one is needed for delivering the required flow. Connecting piping and control and power cables are all below the grating at 279 ft. Therefore they are protected from falling debris.

3A.4.2.2 Boration Using Refueling Water

The reactor coolant system can be borated also by using refueling water. This boration process is slow because of the low boric acid concentration in the refueling water. As a result, a process of feed and bleed is required. For this, the following components are needed:

1. Volume control tank.
2. Associated piping.
3. Nonregenerative heat exchanger.
4. Refueling water storage tank.(RWST)
5. Component cooling system components.
6. Service water (SW) system components.

The volume control tank is located in the auxiliary building on the intermediate floor.

The letdown station, including the nonregenerative heat exchanger, associated piping, and cables, is located below the operating floor of the auxiliary building. The letdown station has a backup in the excess letdown line and excess letdown heat exchanger located inside the containment. The piping which connects the charging pumps to the volume control tank is located in the auxiliary building below elevation 253 ft 6 in. The refueling water storage tank (RWST) has approximately one-half of its volume below the operating floor of the auxiliary building.

Only if boration is performed by using the refueling water is the component cooling system necessary to provide cooling to the nonregenerative heat exchanger. The system includes the following components.

1. Component Cooling Pumps
2. Component cooling heat exchangers.
3. Component cooling surge tanks.
4. Component cooling valves and piping.

Two component cooling pumps are located in the auxiliary building, southeast side, on the operating floor at elevation 271 ft. The distance between the two shafts is about 10 ft. The same distance exists between the other components, as shown in Figure 7, Sheets 1 and 2.

Equipment/system redundancy and separation and the ample time available for repair give reasonable assurance that the boration function can be performed.

3A.4.3CONTAINMENT VENTILATION SYSTEM

In order to guarantee the satisfactory operation of the instrumentation and control systems required for hot shutdown, the containment air temperature must be maintained at a tolerable level. The ventilation system again requires operation of the service water (SW) and electrical systems. Electrical power is supplied separately from bus 14 to two fans, and from bus 16 to the other two fans via an underground tunnel. Local control is performed by four transfer switches and pushbuttons located in the intermediate building at 253 ft 6 in. floor elevation.

Redundancy and physical separation ensure the containment ventilation function.

3A.4.4EMERGENCY POWER SUPPLY SYSTEM

The emergency power supply system includes the following components:

1. Switchgear.
2. Emergency buses.
3. Two diesel generators.
4. Two diesel fuel-oil storage tanks.

Switchgear and emergency buses at 480 V are needed to carry the power for previously mentioned components. (Two redundant emergency buses are provided.) Bus 14 is located in the auxiliary building, on the operating floor, and bus 16 is on the intermediate floor of the same building. Buses 17 and 18 are located in the screen house, as mentioned in Section 3A.4.1.3.

Each of the two diesel generators is able to supply the emergency power through an independent system of buses (buses 14 and 18 to one diesel generator, and buses 16 and 17 to the other diesel generator).

Credit is not taken for redundancy from offsite power supply since total loss of offsite power has been assumed. This is an extremely conservative assumption since the switchyard is located 2500 ft south of the plant and the connecting cables are run underground.

The two diesel fuel-oil storage tanks are 6 ft below grade and the pipelines run underneath the hydrogen storage building.

Redundancy and physical separation give reasonable assurance that emergency power will be supplied.

3A.4.5CONTROL SYSTEM

3A.4.5.1Control Room

The shutdown operations are directed from the control room located on the southeast side of the turbine building. A redundant means of maintaining the plant in hot shutdown condition is provided by local control of the vital components and a local panel that displays the steam generator and pressurizer level and pressure, as described in Section 3A.4.5.3.

3A.4.5.2Systems of Batteries

Each of the two separate systems is able to carry its expected shutdown load. Their location is two floors below the control room.

Cables feeding the dc loads are protected since one cable unit runs in an underground duct bank.

3A.4.5.3Steam-Generator Level and Pressure Indicators, Pressurizer Pressure and Level Control

A local panel in the intermediate building gives indication of the above instruments. Cables from the containment to the panel are run in an underground tunnel.

Proper functioning is also required for the following components which are protected from tornado loads:

1. Communication network between the local panel and the components which have to be operated (boric acid transfer pumps and charging pumps) is provided by a paging system.
2. Pressurizer heaters are required to maintain heat removal by natural circulation. Their location is inside the containment; thus, no additional protection is required. The power supply is from buses 14 and 16 in the auxiliary building. Local control is provided on the intermediate floor of the auxiliary building.

Redundancy, physical separation, and proper location give reasonable assurance that the plant will be under control during and after a tornado.

3A.5 TORNADO EFFECT ON SPENT FUEL POOL

The spent fuel storage pool is located in a structure attached to the end of the auxiliary building and adjacent to the containment, as shown in Figures 8 and 9. The pool itself is 43 ft long, 22 ft 3 in. wide, and 40 ft 3 in. deep. The superstructure could blow outward as a result of a direct hit by a tornado. No damage would result to the pool itself, however, because of the thick concrete biological shield walls and the location of the pool at a low elevation.

The only conceivable means for water loss would be due to action of tornado winds on the pool during the incident time interval.

It is possible for tornado action to cause a partial water loss. It is somewhat speculative, however, that tornado action could empty a pool of the depth and restricted dimensions of the spent fuel pool (SFP). Because of the depth of the water in the pool and friction on the walls of the pool and the spent fuel assemblies and their storage racks, it is not anticipated that a tornado could completely uncover the fuel assemblies. Approximately 68% of the pool water could be removed without uncovering the top of the fuel assemblies. Assuming water remains only at the top level of the fuel assemblies and that the pit holds one-third of a core which has decayed 1 week after refueling, it would take over 3 hr to heat the water from its normal temperature to 212°F.

The assumed heat load would cause the water to boil off at a rate of 3.2 in./hr. Thus it would take approximately 18 hr before the level could reach the midplane of the assemblies.

The two fire pumps can be arranged to reflood the pool at a rate of 6 in./min.

APPENDIX 3B

DESIGN OF LARGE OPENING REINFORCEMENTS FOR CONTAINMENT VESSEL

SEPTEMBER 6, 1968 GAI REPORT NO. 1683

R. E. Ginna Nuclear Power Station

J. D. Riera, Ph.D.
D. K. Croneberger
K. E. Nodland

Including

3B Appendix A	EFFECT OF CONCRETE CREEP AND THE SUSTAINED OPERATING STRESSES ON STRESS DISTRIBUTION AROUND OPENINGS IN A RAPIDLY PRESSURIZED REINFORCED CONCRETE VESSEL
3B Appendix B	EARTHQUAKE ANALYSIS
3B Addendum	ADDENDUM TO THE REPORT ON: DESIGN OF LARGE OPENING REINFORCEMENTS FOR CONTAINMENT VESSEL

TABLE OF CONTENTS

SUMMARY

I. DESIGN BASES

The large openings consisting of a 14 ft 0 in. diameter opening (equipment access hatch) and a 9 ft 6 in. diameter opening (personnel lock) are designed generally in accordance with the criteria outlined in Section 5.1.2.3 of the Final Description and Safety Analysis Report. The only substantive difference relates to the fact that the principal mild steel reinforcement used in the vicinity of the openings has a 60,000 psi, in lieu of 40,000 psi, yield stress. There is no mix of rebar types for principal reinforcement in the high stress area.

II.GENERAL DESCRIPTION

The vertical prestressing tendons are draped around the holes and are continuous (i.e., no tendons are terminated at the hole). Elliptical rebar rings are located around the hole as principal reinforcement. Where practical, hoop rebars are draped around the opening. Radial rebars are provided to the extent required by calculated radial (to the hole) stresses. Normal shear forces, due to pressure on the hatch, at the interface between penetration barrel and concrete are resisted by steel shear rings.

III. STRESS DISTRIBUTION AROUND A CIRCULAR HOLE IN A CIRCULAR CYLINDRICAL SHELL

As described in more detail in Section 3 of GAI Report No. 1683 (hereafter called the report), a survey was made of the available theoretical solutions and experimental techniques for determining stress distributions around circular holes in a shell structure. This survey indicated that an available programmed finite-element solution was superior for this application.

IV. ANALYSIS OF STRESSES AROUND LARGE OPENINGS

A. Method of Analysis

The adequacy of the design of the openings was verified by the use of Computer Program FELAP developed at Franklin Institute Research Laboratories (FIRL). This program provides for the representation of the shell by flat rectangular panels with multiple layers and is used on the assumption that the perturbation on the shell introduced by the presence of the opening is local. The basis for the derivation of this program is described in Reference 13 to the report.

B. Verification of Method Accuracy

In order to evaluate the accuracy of the solution method, a test problem was solved to develop stresses which could be directly compared with other theoretical solutions and experimental results. Very satisfactory results were obtained as evidenced by the data presented in Section 4.1 of the report. This study further verified the adequacy of the grid used on the analysis of the openings for the R. E. Ginna Containment Vessel.

C. Basis for Analytical Model

For purposes of the analysis the shell was idealized by representing (1) the liner as an isotropic steel layer, (2) the horizontal reinforcement as an orthotropic layer with no Poisson's ratio effect and no shear or meridional stiffness, and (3) the elliptical ring

reinforcement with zero shear stiffness, the hoop stiffness varies from zero along the horizontal axis of the opening to the maximum value along the vertical axis and the meridional stiffness varies in the converse manner. A more complete description of the model idealization is contained in Section 4.3.1 of the report.

The effect of concrete cracking was established by setting the stiffness coefficient normal to the crack equal to zero. This procedure was followed for the factored accident pressure of 90 psi and no thermal effect which is the most unfavorable condition. A more detailed description of the cracking criterion and its application is contained in Section 4.3.3 of the report. Sufficient steps in crack development were evaluated to confirm reasonable convergence requirements. The significant conclusion was reached that the distribution of stress-resultants and stress-couples was rather insensitive to such variations as changes in shear modulus of cracked concrete as well as the degree of cracking.

D. Load Combinations

The basic loads including dead, internal pressure, earthquake, prestress, thermal (operating and accident) loads were combined in accordance with the basic criteria and as more fully tabulated in Table 4-1 of the report. An additional possible loading condition investigated involved the stress redistribution resulting from the hypothesized loss of bond along the horizontal rebars terminated near the edge of the opening. All loading conditions are more fully described in Section 4.3.2 of the report.

E. Non-Linear Effects

The effect of load redistribution due to concrete shrinkage and creep was investigated as described in Section 4.3.4 of the report and found to be negligible.

F. Summary of Results

The stress-resultants and stress-couples for panels which were found to be of interest in evaluating the adequacy of the design are summarized in Tables 4-2 and 4-3. The correctness of the values computed by the finite-element method was verified in several ways, as described in Sections 4.1 (c) and 4.3.3 of the report.

V. VERIFICATION OF REINFORCEMENT ADEQUACY

A. General Method

Principal stress-resultants and stress-couples were computed and found to be colinear or essentially so for all panels which were significant in the design check. Likewise the orientation of stress-resultants and stress-couples was found to essentially coincide with the mild steel reinforcement for all significant panels. Interaction diagrams were prepared based upon procedures for ultimate strength design of ACI 318-63. Interaction diagrams for those panels found to be significant are included as Figures 19 through 24 of the report indicating the stress state for all pertinent loading combinations. The interaction diagrams show that sufficient reinforcement has been provided to carry all loads, including the full thermal stress-resultants and stress-couples.

B. Additional Considerations

Additional studies were performed to evaluate the acceptability of liner stresses (assuming total composite action), penetration barrel, reinforcement for normal shears, mechanical

anchorages for terminated rebar and tendon friction losses all of which are described in Sections 5.4 through 5.9 of the report.

C. Design Drawings

Design drawings providing details of the opening reinforcement are included at the end of the report.

1. DESIGN BASES

1.1GENERAL

The large openings in the Containment Vessel are designed generally in accordance with the criteria outlined in Section 5.1.2.3 of the Robert E. Ginna Nuclear Power Plant Final Description and Safety Analysis Report (FSAR), and as more completely detailed hereafter. The large openings consist of the opening for the equipment access hatch with a diameter of 14 ft 0 in. and the opening for the personnel lock with a diameter of 9 ft 6 in. Although these criteria and the analytical and design methods described hereafter apply to both openings, detailed results are provided only for the larger opening.

1.2DESIGN LOADS

The following loads were considered in the structural design of the Containment Vessel:

a. Test Pressure - 69 psig (1.15 times design pressure)
b. Accident Pressure - Design Pressure is 60 psig
c. Thermal Loads
    1. Accident
    2. Operating
    3. Test
d. Seismic Ground Accelerations
e. Dead Load
f. Prestressing Load

The thermal loads on the Containment Vessel and their variation with time are developed on the basis of the blow-down transients shown in Figures 14.3.4-2 and 14.3.4-3 of the FSAR. The openings as a portion of a Class I structure are designed on the basis of a ground acceleration of 0.08g acting in the horizontal and vertical planes simultaneously as the design earthquake and of 0.20g acting in the horizontal and vertical planes simultaneously as the maximum hypothetical earthquake.

The equipment access hatch consists of a single door located outboard of the containment shell with a personnel lock inset in the door. The barrel (penetration sleeve) for the hatch is consequently subjected to the accident pressure. The isolated personnel lock consists of double doors, one located inboard and the other outboard of the containment shell. The design considers the consequence of both doors being closed during the accident as well as the extremely remote possibility that either one of the doors is opened during the accident.

1.3LOAD COMBINATIONS

The design is based upon limiting load factors which are used as the ratio by which dead, accident, and earthquake loads are multiplied for design purposes to ensure that the load

deformation behavior is essentially elastic. The loads utilized to determine the required limiting capacity of any structural element are computed as follows:

a. $C = (1.00 \pm 0.5)D + 1.5P + 1.0T$

b. $C = (1.00 \pm 0.5)D + 1.25P + 1.0T' + 1.25E$

c. $C = (1.00 \pm 0.5)D + 1.0P + 1.0\underline{T} + 1.0E'$

Symbols used in the above equations are defined as follows:

C: Required load capacity of section

D: Dead load of structure

P: Accident pressure load - 60 psig

T: Thermal loads based upon temperature transient associated with 1.5 times accident

T ′: Thermal loads based upon temperature transient associated with 1.25 times accident pressure.

$\underline{T}$: Thermal loads based upon temperature transient associated with accident pressure.

E: Seismic load based upon 0.08g ground acceleration.

E ′: Seismic load based upon 0.20g ground acceleration.

Refer to Section 5 1.2.4 of the FSAR for acceleration response spectra and structural damping.

The maximum temperature within the Containment Vessel under normal operating conditions will be 125°F.

The equipment access hatch is housed outside of the containment shell within an unheated concrete enclosure provided for biological shielding. It is assumed that the minimum ambient temperature within this enclosure is -10°F. The isolated personnel lock is housed outside of the containment shell within the Intermediate Building. It is assumed that the minimum ambient temperature within this building is 50°F.

For Load Combination "a" (i.e., C = 0.95D + l.5P + 1.0T), the maximum temperature of the inner surface of the liner (inner face of the metal sheet covering for the insulation where the liner is insulated) is calculated to be 312°F. For this load combination the ΔT of the liner where it is insulated at the time of maximum accident pressure is calculated to be 2°F, although the design is based upon a ΔT of 10°F.

1.4MATERIAL STRESS/STRAIN CRITERIA

a. Concrete Reinforcement

The deformed bars used for concrete reinforcement in the Containment Vessel are normally intermediate grade billet steel conforming to either ASTM A15-64 or A408-62T, depending upon the bar size, with a guaranteed minimum yield strength of 40,000 psi. Where required due to stress concentrations in the vicinity of the large openings, the deformed bars used for

concrete reinforcement are made from new billet steel, conforming to ASTM A432-66 with a guaranteed minimum yield strength of 60,000 psi.

The design limit for tension members (i.e., the capacity required for the factored loads) is based upon the yield stress of the reinforcing steel. No mild steel reinforcement is designed to experience strains beyond the yield point at the factored loads. The load capacity so determined is reduced by a capacity reduction factor "ϕ" which provides for the possibility that small adverse variations in material strengths, workmanship, dimensions, and control, while individually within required tolerances and the limits of good practice, occasionally may combine to result in an under-capacity. The coefficient "ϕ" is 0.95 for tension, 0.90 for flexure, and 0.85 for diagonal tension, bond and anchorage.

b. Prestressing Tendons

The steel tendons for prestressing consist of 90 1/4-in. diameter wires using a BBRV anchorage system and high tensile, bright, cold drawn and stress-relieved steel wires conforming to ASTM A421-59T, Type BA, "Specifications for Uncoated Stress-Relieved Wire for Prestressed Concrete" with a minimum ultimate tensile stress of 240,000 psi.

The steel tendons are stressed during the post-tensioning operation to a maximum of 80 percent of ultimate strength and locked-off for an initial stress of 70 percent of ultimate strength. The maximum effective prestress is determined taking into consideration allowances for the following losses, which are deducted from the transfer prestress:

1. Elastic shortening of concrete
2. Creep of concrete
3. Shrinkage of concrete
4. Steel relaxation
5. Frictional loss due to intended or unintended curvature of the tendons

In no event does the effective prestress exceed 60 percent of the ultimate strength of the prestressing steel or 80 percent of the nominal yield point stress of the prestressing steel, whichever is smaller. The design is based upon the steel tendons not being stressed beyond the yield point as defined by ACI 318-63 when subjected to the factored loads.

c. Structural Concrete

The structural concrete will have a minimum compressive strength of 5,000 psi in 28 days. Under operating conditions the allowable concrete stresses are in accordance with ACI 318-63 Part 1V-A, "Structural Analysis and Proportioning of Members-Working Stress Design," and Part V, Chapter 26, "Prestressed Concrete."

The Containment Vessel, including the large openings, is checked for the factored load combinations and compared with what is generally defined as the yield strength of the structure. For concrete, the yield strength is defined except as described hereafter by the allowable stresses given in ACI 318-63, Part IV-B, "Structural Analysis and Proportioning of Members - Ultimate Strength Design." Concrete cracking is assumed when the principal tensile stress based upon all loads including thermal loads exceeds $6\sqrt{f'_c}$ or 424 psi.

d. Liner

The liner is designed as participating with the concrete shell in carrying membrane forces (See 5.1). The stress limits established for the liner are consistent with those limits for stress intensity (i.e., the difference between the algebraically largest principal stress and the algebraically smallest principal stress at a given point) defined in Section III of the ASME Boiler and Pressure Vessel Code and based upon a working strength design consistent with that code.

The liner is carbon steel plate conforming to ASTM A442-60T Grade 60 modified to ASTM A300. This material has a minimum yield stress of 32,000 psi and a minimum ultimate tensile strength of 60,000 psi. The liner plate is normally 3/8 in. thick in the cylinder portion of the structure. In the immediate vicinity of the large openings, this liner plate is reinforced with a doubler plate. The barrel and doubler plate are carbon steel conforming to ASTM A516 Grade 60 Firebox Quality modified to ASTM A300. This material has a minimum yield stress of 32,000 psi and a minimum ultimate tensile strength of 60,000 psi.

1.5TEST CONDITION

No specific stress or strain limits are established for the test condition. The factored load combinations previously described have been established so as to ensure that the response due to design loads is essentially elastic. A check is made to ensure that no significant permanent deformation of the structure occurs during the test. This means that following the test there should be no visible permanent distortion of the liner and only small hairline cracks should exist in the concrete.

1.6OPERATING CONDITION

The load combinations relevant to operating conditions are determined as reflected in Section 4.3.2 of this report. Allowable stresses are based upon those stipulated in ACI 318-63.

2. GENERAL DESCRIPTION OF OPENING REINFORCEMENT

2.1INTRODUCTION

The normal flow of stresses in the hoop and meridional direction is obstructed by the large access holes in the Containment Vessel. During normal operation of the plant, vertical prestress forces are the single largest stress contributor. These forces do not create any difficulty in transferring vertical compressive stresses around the opening, but give the necessary reserve compressive stresses to counterbalance the vertical strains resulting from the accident pressure load. The horizontal stresses in the hoop reinforcing steel are very small during normal operation, but will theoretically increase up to almost yield stress due to the factored pressure load. These hoop forces will be transferred around the opening by draped continuous hoop reinforcing steel, and elliptical ring reinforcing steel.

2.2REBAR FOR DISCONTINUITY STRESSES

As seen from Drawing No. D-421-023 (Figure Drawing 2), some of the hoop reinforcing bars are terminated at the opening. The tensile load in these bars is transferred to the concrete by bond, or through the end anchor plates, or a combination of both. The effect of these different conditions was carefully investigated.

The elliptical ring reinforcing steel will be spliced by use of a Cadweld Rebar Splice. These splices are located at points of low rebar stresses, and no more than 1/3 of the ring steel will be spliced in one section. This should eliminate any slip between Cadweld and rebar that could occur at high rebar stresses.

Radial tensile stresses out from the center of the access opening are created due to the pressure load. Radial reinforcement is provided to carry these stresses out from the opening and will be terminated where "pure" membrane stresses exist in the wall.

2.3NORMAL SHEAR AT EDGE OF OPENING

The peripheral or normal shear reinforcement in the concrete around the Penetration Barrel is designed for the computed shear at equal distance or greater than, d/2 = 33.0 in., from the edge of the opening per ACI 318-63, or for twice the normal shear due to internal pressure on the hatch, whichever is the larger of the two values.

2.4PRESTRESSING

The vertical tendons will be curved around the opening, using a minimum radius equal to 20.0 feet. The total angular change of the tendons was laid out to keep the frictional losses within a satisfactory margin, and to satisfy a practical execution of the job in the field. However, it will be required to retension all the curved tendons around the large access openings approximately 1000 hours after the initial stressing. The minimum effective prestress after 40 years, i.e., the lifetime of the plant, will then be met.

3. STRESS DISTRIBUTION AROUND A CIRCULAR HOLE IN A CIRCULAR CYLINDRICAL SHELL

3.1INTRODUCTION

The first theoretical treatment of the problem presented by openings in thin shell structures is commonly attributed to Lur′e[1], who obtained an approximate solution for the stress distribution around a very small circular cut-out in a thin circular cylindrical shell subjected to a homogeneous biaxial stress state σ_x' σ_θ. Lur′e derived the following expression for the edge stress:

$$\sigma = (\sigma_x + \sigma_\theta) - 2(\sigma_x - \sigma_\theta)\cos 2\phi$$

$$+\sqrt{3(1-\nu^2)}\,\frac{\pi d^2}{16Rt}\,[2\sigma_x + (\sigma_\theta - 3\sigma_x)\cos 2\phi] \qquad \text{(Equation 3.1)}$$

in which:

σ_x = meridional stress in the shell without the opening

σ_θ = hoop stress in the shell without the opening

ϕ = angular coordinate (see Fig. 2)

R = shell radius

t = shell thickness

d = diameter of cut-out = 2r

Equation (3.l) does not include bending effects, which can be quite important in thin shells. Therefore, Lur′e's solution represented a relatively minor the flat plate solution[2]. In fact, for many years the design of reinforcement around shell openings was based on the classical stress concentration factors of flat plate theory. In this area solutions for openings reinforced by means of a symmetrical circular doubler plate were obtained by Sezawa and Kubo[3], Gurney[4], and Beskin[5]. Solutions for the stress distribution around unreinforced and ring-reinforced holes in flat plates can be found in Savin's[6] extensive treatment of the subject.

The plane stress approach is not satisfactory, however, for large openings. In this case large stress-couples may appear around the edge of the opening even when the shell elsewhere is in a pure membrane state of stress. Fortunately, very valuable results have recently become available. Withum[7] investigated the stress distribution in a cylinder weakened by a hole, subjected to torsion, by using a perturbation scheme. This technique was extended by Kline 'et al'[8] to determine the stresses around a circular cut-out in a pressurized circular cylindrical vessel. This work, carried out at the General Technology Corporation with the support of the Bureau of Ships of the U. S. Navy, was part of a systematic theoretical investigation of two problems:[9,10]

a. determination of the state of stress in the vicinity of a circular hole on a circular cylindrical shell subject to internal pressure

b. determination of the stress distribution in two normally intersecting cylindrical shells

The solution of problem (a), for internal pressure as well as other practical loading conditions, has been presented by Naghdi and Eringen[10]. Lekkerkerker[11], extending Lur′e's approach, solved the same problem for axial tension and torsion. They found excellent correlation between their solution and experimentally determined stresses (using electric resistance strain gages) in a mild steel tube subject to torsion. Stress concentration factors from Ref (8) to (11) are presented in Figures 1 and 2. The coefficients given may be directly applied to the calculation of maximum stresses at the edge of the opening.

Unfortunately, no theoretical solution is available for reinforced openings or for non-isotropic shells (e.g., orthotropic reinforced concrete shells). The complexity of these problems is such that they can only be dealt with by means of numerical or experimental methods. Among the many possible approaches, the finite-element method and the stress-freezing technique of three-dimensional photoelasticity have become especially attractive in recent years and are briefly evaluated in Sections 3.2 and 3.3.

3.2FINITE ELEMENT METHOD

Steady progress in the finite element approach has led to the possibility of determining the stress distribution around reinforced openings in shell structures with good accuracy. The most important advantage of this method is its generality: reinforcing rings, variable shell thickness and material orthotropicity, for example, may be incorporated into the analysis without difficulty. Unfortunately, the accuracy of the solution must still be evaluated by test: for instance, results obtained using two different grid may provide an indication of convergence. Alternatively, results obtained using a prescribed grid size and pattern may be checked against some of the theoretical solutions of Section 3.1 or against experimental values. The latter approach was followed in connection with the analysis of the stresses around the openings for the R. E. Ginna Containment Vessel.

The designs of the reinforcement around the openings in the R. E. Ginna Containment Vessel were verified by using Computer Program FELAP[12], developed at Franklin Institute Research Laboratories (FIRL) The solution is based on a representation of the shell as an assembly of flat rectangular panels. In the first order shell theory described by Zudans[13], which formed the basis for the FIRL finite element solution, the rotation about the normal to the shell middle surface is taken equal to zero. Consequently, this leaves only five degrees of freedom associated with each nodal point. It must be noted that the model with five degrees of freedom at a corner point, while "compatible" for plate problems, is unbalanced for shell problems in the third rotation[14]. Although usually this unbalance does not affect the accuracy of the solution, it can lead to unrealistic results[14]. Therefore, in applications to nuclear power plants, a verification of the results becomes desirable.

Connor and Brebbia[15] developed a stiffness matrix for a thin shell element of rectangular plan and also noted that good results can be obtained with the finite element method using

noncompatible displacement expansions, which do not include all the rigid body displacements[15]. According to Connor and Brebbia[15], it appears that curved elements lead to better results, for the same element size and shape, and are therefore more efficient than flat elements. However, comparison of results obtained using two different types of curved triangular elements[16,35] with flat elements[12,14] for the test problem discussed in Section 4.l did not substantiate that belief (See Figure 9). In fact, all finite-element results were close to Eringen, Naghdi, and Thiel's[9] solution, which can be considered, within the limitations of shallow shell theory, an "exact" solution.

3.3APPLICATIONS OF THREE-DIMENSIONAL PHOTOELASTICITY

Until very recently, experimental methods constituted the only feasible approach to the stress analysis of geometrically complicated reinforced openings in shell structures. In this area, the stress-freezing technique of three-dimensional photoelasticity appears to be the most suitable experimental method. Outstanding studies of stresses around reinforced openings in pressure vessels were carried out by Leven[17], Taylor and Lind[18], and Takahashi and Mark[22]. In the latter, comparison of the photoelastic results with a finite element analysis of the axisymmetric thick-walled reinforced concrete vessel showed very close agreement between the two solutions. Durelli, del Rio, Parks, and Feng[19] carried out an experimental evaluation of the stress around an opening in a thin shell by means of brittle coatings, electrical and mechanical strain gages, micrometers, and photoelasticity with the objective of comparing the accuracy and advantages of each technique.

Photoelasticity was concluded to be the most effective experimental approach in this type of problem[19]. In the fabrication of the model Durelli 'et al'[19] used a Hysol 4290 epoxy resin which was found to give poor performance in recent tests[20]. Mark and Riera[20] believe that the use of improved model materials will lead to a considerable reduction in the dispersion of photoelastic readings, which was large in the past[25], and which still is the most important argument against this experimental approach. In spite of the difficulties associated with the model material, the photoelastically determined stresses in Reference (19) show good correlation with Eringen and Naghdi's[9] theoretical solution. Stress concentration factors determined photoelastically by Durelli 'et al' and by Houghton and A. Rothwell[21] by means of electric resistance strain gages mounted on circular cylindrical aluminum shells are given in Figure 3C. Figure 3C also shows the stress concentration factors computed by Eringen and Naghdi[9].

The photoelastic approach presents several advantages[24]: 1) full field observations give clear understanding of overall behavior and permits recognition of unsuspected critical regions, 2) measurements are made with very small effective gage lengths so that high gradients can be studied in small models, and 3) basic instrumentation is simple and inexpensive. Traditionally, models have been machine finished, but improving casting techniques have already permitted the fabrication of complicated models without any noticeable edge effect. This represents two important steps forward: 1) model fabrication cost can be drastically reduced and 2) the technique may now be applied to complicated models that cannot be readily machined.

Ducts for prestressing "tendons" have successfully been incorporated into epoxy models by using nylon piano cords, which are set in the model prior to casting as if they were rebars in a conventional reinforced concrete element[23]. After the epoxy has hardened, they can be easily pulled out, leaving a perfect duct without residual stresses around the walls. The photoelastic method, therefore, offers the possibility of determining in one single study the stresses around openings in prestressed vessels in "the large", as well as in "the small". The latter, which includes stresses around curved tendons, corners, possible non-linear distributions through the wall thickness, etc., may demand separate analyses when a solution based on thin shell theory is used as the basis for design. On the other hand, in applications for design purposes, the photoelastic method presents some drawbacks: 1) a procedure to include the liner and steel rebars into the model has not yet been proposed. 2) the approach is not adequate for vessels that may be in a cracked condition, such as the R. E. Ginna Containment Structure, which has only vertical prestress (See Section 4.2). Strictly speaking, the method is applicable only to fully prestressed vessels in which virtually no cracking due to high concrete tensile stresses is expected.

Further progress in theoretical or numerical analysis of stresses around shell openings, which must account for non-linear distributions through the shell thickness near the opening and for other effects that cannot be predicted by thin-shell theory, can be fostered by adequate experimental verification of the results, or by purely experimental studies that may help define the areas that require additional investigation. This is illustrated by a photoelastic investigation of stresses around reinforced openings in plates due to Lerchenthal[27], which indicates that the departure from a plane stress distribution near the openings may be significant. For this purpose, the stress-freezing technique may yet prove to be an invaluable tool.

4. ANALYSIS OF THE STRESSES AROUND LARGE OPENINGS IN THE R. E. GINNA SECONDARY CONTAINMENT VESSEL

4.1VERIFICATION OF FINITE-ELEMENT METHOD OF ANALYSIS

As outlined in Section 3.1, a finite element solution was chosen to determine stresses around large openings in the containment vessel. The selection of this approach was based on an overriding consideration: it constitutes the only method by which the steel reinforcement around the opening as well as the orthotropic character of the shell in the cracked condition (see Section 4.2) can be taken into account. To evaluate the accuracy of the solution method (FIRL Program FELAP, as described in Section 3.2), a test problem was solved with the same grid used in the finite-element analysis of openings for the R. E. Ginna Containment Vessel. The grid is shown in Figure 4. In the finite element analysis the following assumptions were made:

a. The perturbation introduced by the presence of the opening on the shell state of stress is localized.

b. According with (a), stresses and displacements some distance away from the region surrounding the opening are not affected by the opening.

c. A panel of rectangular plan, which is centered around the opening, is removed from the shell (Figure 4). The displacements corresponding to the shell without the opening along the boundary lines of this panel constitute the boundary conditions for the finite-element analysis. The analysis is correct if the panel boundaries are sufficiently far from the opening so that (a) and (b) apply. This assumption can be verified 'a posteriori' by comparing stresses along the boundary lines with those existing in the shell without the opening.

d. Because of symmetry, only one quadrant need be analyzed.

Since reliable experimental or theoretical results for reinforced openings in shells similar to that under consideration were not available, it was decided to check the solution method against the shell tested by Durelli 'et al'[19], for which other theoretical solutions were also available. The problem is defined by:

R = 430.00 in.

r = 85.70 in.

t = 18.04 in.

ν = 0.30

p = 100.00 psi

The computed tangential membrane stresses around the opening edge are compared in Figure 5 with those given in Ref. (9) and with the experimental stresses determined by Durelli 'et al'[19] Similarly, Figure 6 shows the tangential surface stresses around the edge. Additional comparisons between the finite element solution and the experimental values are given in Figures 7 and 8. Finally, Figure 9 shows the variation along the symmetry axes of the stress resultant N_θ determined by different approaches, including another finite-element solution

using triangular shell elements based on Prato's work[16]. The correlation of the FIRL finite element solution with the other results is good. It must be noted that the finite-element results are particularly close to the solution of Eringen 'et al', which was regarded as the most accurate. It should also be pointed out that the correlation is good in spite of the fact that the panel boundaries were not sufficiently removed from the opening, as revealed by Figure 8 which

shows the existence of a small stress couple M_θ at $\frac{s}{r} = 3.5$ that had not been predicted by the model study. This result was verified by another finite-element analysis of the test problem using Prato's triangular shell elements[16].

It was pointed out in Section 3.1 that the stress concentration factors under loading conditions such as internal pressure, axial tension or torsion can be computed at different locations in terms of the nondimensional parameter (See Figure 2). As $\nu \rightarrow 0$ we approach the plane stress solution and the convergence problem for the finite-element solution disappears. It can be concluded, therefore, that satisfactory results in the test problem ($\nu = 1.17$) constitute adequate verification of the solution method for the large openings in the R. E. Ginna Containment Vessel for which $\nu = 0.62$ (equipment hatch, based on typical shell thickness).

4.2GENERAL CONSIDERATIONS CONCERNING METHODS OF ANALYSIS OF REINFORCED CONCRETE STRUCTURES IN THE CRACKED CONDITION

The stress distribution in reinforced or prestressed concrete shell structures subject to cracking may be approximately determined by analyzing the shell with appropriately reduced stiffness coefficients. Milekykovsky and Hedgren and Billington[29] used the method to obtain approximate solutions for reinforced concrete cylindrical shells in the post-linear range. In order to eliminate the uncertainty related to the somewhat arbitrary reduction of stiffness coefficients in the above analyses[28,29] Riera and Billington[30] proposed to assume that the concrete-reinforcing steel composite material is non-linearly elastic, which is shown to be an adequate idealization for concrete shell roofs under sustained loads.

Following a different but essentially parallel approach, Rashid[31] proposed to treat the influence of a crack on a continuous element as a mechanism that changes the element's behavior from isotropic to orthotropic. In other words, concrete is assumed to be isotropic whenever stresses are contained inside the failure surface. It becomes orthotropic when a crack develops normal to a principal stress direction. The stiffness coefficients are then set equal to zero in the direction of the normal to the crack. Once a cracking criterion is established, practical solutions can be obtained using a discrete representation, or a finite-element formulation of the problem. An essentially identical procedure used by Watson to determine stresses around a circular tunnel through a rock material with a stringent cracking criterion is briefly described by Zienkiewicz[32].

Several areas of concern associated with the approach may be mentioned: First, the failure surface for concrete and its time and temperature dependence have not yet been well defined. Disagreement exists concerning the short-time failure envelope of concrete in biaxial compression and to a greater degree concerning general stress states involving at least one principal tensile stress. Second, the question of existence of solutions and convergence of

iterative or other numerical techniques used to determine those solutions have not been explored in depth.

Zienkiewicz[32] notes, in connection with direct iterative solutions for non-linear elastic materials, that three or four iteration cycles are usually sufficient to obtain satisfactory results. Riera and Billington[30] also obtained good correlation between experimental and numerical results for a cylindrical reinforced mortar shell after three iteration cycles, but they note that the process is not necessarily convergent and that there is no rigorous justification for using the values obtained after a few iteration cycles, disregarding what may happen afterwards. Since the convergence of the iterative procedure depends upon the degree of nonlinearity of the constitutive equations, the problem may be circumvented by applying the loads in small increments[30]. The question of how small these increments should be still remains unresolved. Rashid[31] determined the load-carrying capacity of axially symmetrical prestressed concrete primary pressure vessels by iterating until no further cracks develop after each small load increment, thereby improving the likelihood of obtaining a correct solution.

In spite of the aforementioned areas of concern, the stress analysis of reinforced or prestressed concrete shells in the cracked condition on the basis of reduced or modified stiffness coefficients has been quite successful. The method also led to valuable results in the stress analysis of thick (axially-symmetrical) pressure vessels. The correlation between experimental and theoretical results reported in Ref. 28 to 31 is good and should encourage additional basic research in this area. In the meantime, the technique appears to be sufficiently developed to be used in the solution of technical problems, such as the stress distribution around large openings in the R. E. Ginna Containment Vessel. Because of the computational effort demanded by the solution of this particular problem, elaborate approaches such as application of the load in small increments, combined with iteration, could not be employed. Instead, a direct iterative technique on the stiffness distribution (with the fully loaded structure) was used. Furthermore, the application of the former method would require the specification of a complete history of external loads and temperatures, which are not known nor easily predictable. In other words, too many loading conditions need be investigated to make the approach feasible or even meaningful.

Consequently, areas of concern such as convergence requirements, influence of cracking criterion, and effect of different loading histories on the theoretical results were given careful consideration in the verification of structural adequacy.

4.3STRESS ANALYSIS IN CRACKED AND UNCRACKED CONDITIONS UNDER OPERATING AND ACCIDENT LOADS

4.3.1Representation of the Shell Around the Opening

The finite-element grid used to solve the test problem (Section 4.1) was also employed to determine the stress distribution around the large openings in the Containment Vessel. The shell was idealized as follows:

a. The liner was represented as an isotropic steel layer (E_{st} = 30,000 ksi, ν = 0.3). Composite action was assumed in the determination of the stress resultants and stress couples.

b. The horizontal steel reinforcement (hoop rebars) was represented as a layer of an orthotropic material having no Poisson's ratio effect, no shear stiffness ($G_{12} = 0$) and no meridional stiffness ($E_1 = 0$). This layer was located at the center of gravity of the hoop reinforcement.

c. The ring steel rebars, providing additional reinforcement around the opening, were represented as a layer located at the center of gravity of the ring reinforcement. The shear stiffness of this layer was set to equal zero ($G_{12} = 0$). The hoop (E_2) and meridional (E_1) stiffnesses vary from $E_1 = E_{st}$, $E_2 = 0$ along the horizontal axis of the opening, to $E_1 = 0$, $E_2 = E_{st}$ along the vertical axis of the opening. In Computer Program FELAP the axes of orthotropicity are oriented in the hoop and meridional directions. Consequently, since the axes of orthotropicity of the ring reinforcement only coincide with those directions in the regions around the opening's vertical and horizontal axes, the following approximation was made: at every panel type the hoop and meridional stiffnesses were directly proportioned to the projected steel area.

d. The concrete layers were idealized as follows:

1. Uncracked concrete
   $E_1 = 4000$ ksi
   $E_2 = 4000$ ksi
   $G_{12} = 1740$ ksi.
   $\nu_{12} = 0.15$
2. vertically cracked concrete
   $E_1 = 4000$ ksi
   $E_2 = 0$
   $G_{12} = 800$ ksi
   $\nu_{12} = 0$
3. horizontally cracked concrete
   $E_1 = 0$
   $E_2 = 4000$ ksi
   $G_{12} = 800$ ksi
   $\nu_{12} = 0$
4. fully cracked concrete
   $E_1 = 0$
   $E_2 = 0$
   $G_{12} = 800$ ksi
   $\nu_{12} = 0$

The shear stiffness G_{l2} of cracked concrete was computed taking into consideration the shear deformation of concrete between cracks, as well as the deformation of the rebars

subjected to dowel action. The contribution of the latter was obtained from "Nelson Manual No. 21", Figure 13, p. 12. The following expression for the shear stiffness of concrete (that would lead to a correct in-place shear stiffness of the entire section) was

derived: $$G_{12} \cong \frac{G}{1+\frac{1}{pL}}$$

in which

G = shear stiffness of uncracked concrete

ρ = ratio of area of steel rebars in dowel action to concrete area.

L = distance between cracks (in.)

Taking

ρ = 0.034 and L = 25 in.

G = $\frac{G}{2.17}$ = 803,000 psi

Analyses based on G_{12} equal to zero, 800 ksi and 1740 ksi indicated that the in-plane stress-resultants and stress-couples are not sensitive to variations in G_{12}.

e. The barrel (penetration sleeve) was represented on contributing, with 50 percent of its area, to the stiffness of the elements adjacent to the openings. In other words, a stiffener of 3/8 in. thickness was included in the model along the periphery of the opening.

Note that although the penetration barrel was incorporated into the finite-element model as explained above, it was not regarded as contributing to the load-carrying capacity of the shell (See Section 5.2).

4.3.2Basic Loading Conditions

The stress distribution around the opening was determined for the loading conditions described in Section 1 and those loading combinations more completely described hereafter. The specific loads are defined as follows:

a. Dead Load

The stress distribution around the opening due to dead weight was calculated assuming a uniform meridional compression in the cylinder equal to the stress resultant at the elevation of the opening axis (in the shell without the opening). The weights of the equipment hatch and personnel lock were neglected. Since dead weight stresses in the typical shell wall at the elevation of the equipment and personnel access are low (less than 100 psi), the above simplifications will not significantly influence the final stresses in the pressurized vessel.

b. Internal Pressure

Internal pressure was assumed to act on the interior of the shell as well as on the barrel (penetration sleeve) of the equipment access hatch. The internal pressure on the hatch was

assumed transferred to the shell by a uniform normal shear Q_ρ around the opening. The effect of non-uniform distributions of Q_ρ were analyzed separately.

The personnel opening was analyzed with and without internal pressure acting on the barrel (penetration sleeve).

c. Earthquake

Seismic stresses around the openings were investigated for two directions of the horizontal component of motion:

1. earthquake motion oriented in the direction normal to the openings
2. earthquake motion oriented at 90° with the direction normal to the openings

Seismic loads were evaluated as described in Appendix B.

d. Prestress

Prestressing loads are represented as two independent loading conditions by a uniform meridional compression in the shell (away from the opening) equal to the stress resultant corresponding to initial and final prestress. Curved tendons around the opening were considered in the analysis as line loads q = T/r where T is the total prestressing force per tendon and r is the radius of curvature at the location under consideration. These line loads were integrated within each panel and applied as nodal forces on the shell, as shown in Figure 11.

e. Thermal Loads

1. Operating Temperature

The steady-state temperature distribution in the reinforced area around the opening was obtained using a modified Gauss-Seidel iteration technique.

The structure was broken up into 2257 elements (38 x 62 nodes) and the temperature at each node was determined by the temperature at the four nodes surrounding it using the formula:

$$T = \frac{\sum_{i=1}^{4} T_i K_i \frac{t_1}{X_i}}{\sum_{i=1}^{4} K_i \frac{t_i}{X_i}}$$

The skin temperatures of the structure were determined by a parabolic curve fit using the formula:

$$h(T_{AMP} - T_{skin}) = -\frac{k}{2\Delta X}(3T_{skin} - 4T_{skin-1} + T_{skin-2})$$

or

$$T_{skin} = \frac{T_{AMP} - \frac{k}{2\Delta Xh}[T_{skin-2} - 4XT_{skin-1}]}{1 + \frac{3k}{2\Delta Xh}}$$

The following values were used for the thermal conductivity:

INSULATION	k = 0.0208 $\frac{BTU}{hr\,ft\,°F}$
STEEL	k = 26.0 $\frac{BTU}{hr\,ft\,°F}$
CONCRETE	k = 0.8333 $\frac{BTU}{hr\,ft\,°F}$

The following values were used for the boundaries:

INSIDE	h = 2.0 $\frac{BTU}{hr\,ft^2\,°F}$
TOP	h = 1.0 $\frac{BTU}{hr\,ft^2\,°F}$
OUTSIDE	h = 1.0 $\frac{BTU}{hr\,ft^2\,°F}$
BOTTOM	Adiabatic

The concrete was considered to be 4 percent steel reinforcement and its conductivity was determined from the formula:

$k_{effective} = .96k_{concrete} + .04k_{steel}$

The iteration was performed on the computer to a tolerance of 0.005°F.

Typical results of the thermal analysis for operating conditions are given in Figure 12, which shows the temperature distribution around the opening for the equipment access hatch with an interior air temperature of 120°F and an exterior air temperature of -10°F. Linearized thermal gradients at 8, 32, and 96 in. from the edge are shown in the same figure.

The input for the finite-element stress analysis was prepared on the basis of the above results. The steady-state (winter) temperature distribution around the opening used in the analysis is indicated in Figure 13. To simplify the input, a temperature of 0°F was used in the analysis for the outside face of the typical wall rather than -3°F. Consequently, all temperatures were shifted by +3°F.

Summer thermal stresses are conservatively computed as equal to 40 percent of the peak winter thermal stresses.

2. Accident Temperature

Since the finite-element solution used in the analysis is restricted to linear temperature gradients through the wall thickness, accident thermal stresses, which result in a highly non-linear gradient, were computed as described below:

a. Effect on typical wall: The 10°F temperature increase in the liner was conservatively represented by an equivalent internal pressure equal to the pressure that the heated liner would exert against a rigid confining cylinder.

b. Effect on the barrel (penetration sleeve): The effect of increasing the liner temperature to 312°F (net increase: 312 - 120 = 192°F) was represented by internal pressure acting on the barrel. The magnitude of this pressure was determined on the basis of a two dimensional analysis, which assumed that the barrel (t = 0.75 in.) plus 0.55 in. of concrete were suddenly heated to 192°F. The equivalent pressure on the concrete was found to be equal to 160 psi.

f. Bond Failure Along Rebars Anchored Near Opening Edge

It is expected that the horizontal rebars terminated near the edge of the opening will transfer their load by bond to the surrounding concrete and thus to the ring reinforcement and adjacent (uninterrupted) rebars. However, since concrete in the area involved may present vertical cracks, it appears unsafe to rely only on bond stress transfer. Therefore, the stress redistribution that would occur in case of a complete bond failure along all horizontal rebars terminated at the opening was investigated as described below.

Figure 14a shows one such rebar with the rebar load before bond failure (as determined by the finite element analysis of the pressurized shell in the cracked condition) indicated in Figure 14b. The assumed bond stress distribution is also shown in Figure 14b. Note that the shaded area times the perimeter of the rebar equals the load in the rebar away from the opening. The applied loads in the finite element study of the stress redistribution due to bond failure are schematically shown in Figure 14c. The stress resultants and stress couples from the present analysis were superimposed with those corresponding to internal pressure to obtain the stress state expected under internal pressure in the case when all loads of the rebars are transferred to the mechanical anchorage at the end of the rebars. These stresses are treated in the evaluation of the results as an independent loading condition. The load combinations considered in the analysis are given in Table 4-1. The stress-resultants, stress-couples and normal shears due to the 76 load combinations described in Table 4-1 were calculated using a computer program for sixteen elements located along both symmetry axes and along a 45° line.

4.3.3Effect of Concrete Cracking

The effect of concrete cracking on the stress distribution around the opening was determined, as outlined in Section 4.2, by assuming that concrete principal tensile stresses in excess of 424 psi produce cracks in the direction normal to that principal stress direction. In the finite

element analysis this is accomplished by setting a stiffness coefficient at that location equal to zero. Since this procedure cannot be performed for every load combination, the iteration was carried on for accident conditions with 90 psi internal pressure and no thermal effect, which appears to be the most unfavorable condition as far as the extent of cracking around the opening is concerned. The shell was first analyzed in the uncracked state, and the stresses corresponding to the following load combination determined:

$$1.0\ DL + 1.0\ VP_f + 1.5\ IP$$

In successive runs the average principal tensile stresses within each of the concrete layers of the model (See Figure 10) were inspected. When this average principal stress at any layer of an element exceeded 424 psi, the elastic properties of that particular layer were changed as follows:

a. If the average principal tensile stress direction is sensibly horizontal, then E_2 is set equal to zero.

b. If the average principal tensile stress direction is sensibly vertical, then E_1 is set equal to zero.

c. If the average principal tensile stress direction is approximately 30°, 45° or 60°, then:

   $E_1 = E_0 \sin 30°$ $E_2 = E_0 \cos 30°$, or

   $E_1 = E_0 \sin 45°$ $E_2 = E_0 \cos 45°$, or

   $E_1 = E_0 \sin 60°$ $E_2 = E_0 \cos 60°$

   respectively. For cracks oriented other than horizontally or vertically, the above stiffness coefficient reduction constitutes an approximation Figure 15 gives the stress-resultant distribution under internal pressure along both symmetry axes for the uncracked shell, as well as results of several analyses for the cracked shell. It should be noted that the difference between stress resultant distributions based on different degrees of cracking is not excessive and, furthermore, that all distributions are close to the distribution corresponding to an uncracked, unreinforced shell computed on the basis of Eringen's 'et al' theory[9]. Whenever possible, the results presented in References (*9*) to (*11*) were compared with the finite-element solutions to provide additional evidence on the correctness of the computed values. Displacements for vertical prestress and internal pressure are shown in Figures 16 and 17.

   Stress-resultants and stress-couples for the uncracked shell can be found in Table 4-2. The results corresponding to the last computer analysis are summarized in Table 4-3. Tables 4-2 and 4-3 give the stresses at the center of the elements located along both symmetry axes and along an approximately 45° line (See Figure 4). Inspection of the data indicates that these elements represent the significant areas which could conceivably control the design.

   These results are considered to represent the state of stress in the shell with the cracking pattern expected under 90 psi internal pressure. Note that these distributions for the basic loading conditions were obtained with the same model. Also note that earthquake stresses were not computed by means of the finite-element technique. (See Appendix B)

4.3.4Effect of Creep and Shrinkage

It appears that shrinkage of concrete can only introduce compressive stresses into the steel rebars. These stresses will largely disappear after cracking due to the internal pressure in the shell takes place, and need not be considered in the stress analysis of the opening.

The load redistribution due to concrete creep (i.e., the redistribution of N_ϕ, $N_{\phi\theta}$, N_θ, M_ϕ, M_θ, etc.) is expected to be small. This conclusion is sustained by a finite-element plane stress analysis, which indicates that the stress concentration factor for uniaxial compression changes by only 5 percent when the hoop 'in-plane' stiffness is reduced by 100 percent. If the 'effective modulus' approach is used to determine the final stress distribution under operating stresses, a final modulus equal to 40 percent of its initial value would lead to a final ratio between vertical and hoop 'in-plane' stiffness equal to:

$$\frac{42 \times 1600}{40.6 \times 1600 + 1.4 \times 30,000} = \frac{42}{66.8} = 0.63$$

the initial ratio is:

$$\frac{42 \times 4000}{40.6 \times 4000 + 1.4 \times 30,000} = \frac{42}{51.1} = 0.82$$

Therefore, a change in the ratio between vertical and hoop in-plane stiffnesses of about 23 percent is not expected to have any significant effect on the stress-resultant and stress-couple distributions.

The effect of creep and shrinkage on prestress losses is taken into account as indicated in Section 5.8. Likewise, the transfer of load from concrete to steel in any given cross-section is considered in the verification of rebar stresses when applicable.

With reference to the discussion of Appendix A, the following conclusions can be stated:

a. The load redistribution due to concrete creep in the unpressurized vessel will not affect in any significant degree the load distribution in the structure under test or accident pressure.
b. The knowledge of the stress-resultant and stress-couple distributions after creep in the unpressurized vessel cannot be of direct use in the evaluation of the corresponding distributions under internal pressure, should the internal pressure be applied late in the life of the structure, since as concrete cracking takes place, the distribution before the internal pressure is applied changes according to the cracking pattern.

5. VERIFICATION OF DESIGN CRITERIA

5.1BASIS FOR VERIFICATION OF SHELL LOADING CAPACITY DUE TO PRIMARY LOADS (PRINCIPAL STRESS-RESULTANTS AND PRINCIPAL STRESS-COUPLES)

The loading capacity at any point of the shell was verified according to the following procedure:

a. The principal stress-resultants N^1 and N^2 were computed in terms of N_ϕ, N_θ, and $N_{\phi\theta}$

b. The principal stress-couples M^1 and M^2 were computed in terms of M_ϕ, M_θ, and $M_{\phi\theta}$

c. Considering that throughout the critical regions of the shell (both axes of symmetry and along the edge of the opening) the orientations of N^1, N^2, and M^1, M^2 coincide with the orientation of the reinforcement and that in the rest of the shell they nearly coincide with each other and with the orientation of the steel rebars, systems N^1, M^1 and N^2, M^2 are treated independently. Since in the regions in which the directions of principal stress-resultants and stress-couples are not colinear or do not coincide with the orientation of the steel rebars, stresses are low, the error introduced by assuming them colinear will not affect the conclusion concerning the load-carrying capacity of the shell. In the latter case, steel rebars not oriented in the direction of principal stress-resultants or stress-couples were conservatively neglected in the computation of the strength of the section. In other words, it is proposed that forces it the 1-direction will not affect the strength of the section in the 2-direction and vice verse. This is in full agreement with a square failure criterion for concrete in biaxial compression, which appears to very conservative. Stresses in rebars oriented along a principal stress direction obviously will not be affected by forces in the other principal direction.

d. The computed ultimate capacity of any section of the shell satisfies the requirements of ACI 318-63, Sections 1600, 1700, 1800, and 1900. 0nly deformed bars as defined in ACI 318-63, Section 301 are used. Deformed bars ensure higher bond strength and a more uniform crack distribution.

e. Composite action between the shell and the liner is neglected in the computation of ultimate moments. The liner is regarded as carrying only its share of the principal stress-resultants.

Interaction diagrams were prepared as described in Section 5.2 for elements located along both symmetry axes and along a 45° line. Principal stress-resultants and stress-couples corresponding to all critical load combinations are show in Figures 19 through 24 on the interaction diagram corresponding to elements 55, 66, 77, 49, 73, 97, and 101. The position of a point representing a stress state within the diagram gives a clear indication of the 'local safety factor' at that location (i.e., at the center of the element). It must be emphasized that even if a point representing a stress state fell outside the diagram, that would not indicate a critical or nearly critical condition for two reasons:

a. The interaction diagrams were determined on the basis of conservative assumptions and it is expected that the 'true' failure envelopes lie a certain distance away from the computed envelopes.

b. A point outside the interaction diagram would merely indicate local yielding of one or more rebars at that location, which would cause a load redistribution towards less highly stressed regions. A point representing a stress state contained withIn an interaction diagram indicates that stresses in all steel rebars at that section are below yield stress, and that concrete stresses, where applicable, are below code allowable stresses.

5.2INTERACTION DIAGRAM

a. Axial Compression and Bending

(See Figure 18)

1. Concentric Compression

$$P_0 = \phi[0.85\ f'_c\ A_c + A_{st}\ f_y],$$

$$A_{st} = A_{s1} + A_{s2} + A_{s3} \quad \text{(Equation 5.1)}$$

2. Simple Bending

$$a = \frac{A_{s1}\ f_y + A_{s2}\ f_{s2} - A'_{s3}\ f_{s3}}{0.85\ f'_c\ b} \quad \text{(Equation 5.2)}$$

$$M_0 = \phi\left[T_1 d_1 + T_2 d_2 + C_{s3}\ d_3' + C_c\left(C - \frac{a}{2}\right)\right]$$

$$\frac{C}{\varepsilon_c} = \frac{d}{\varepsilon_{st} + \varepsilon_c}$$

$$C_c = 0.85\ f_c'\ a\ b$$

3. Bending and Axial Compression

$$C_b = \frac{d(87000)}{87000 + f_y}$$

$$a_b = k_1\ a.b \quad \text{(Equation 5.3)}$$

$$P_b = \phi\ [0.85\ f_c'\ (a_b - a)\ b]$$

$$M_b = M_0 + P_b\, d_b$$

4. Determine P_a and M_a

$$e_a = 0.1\ t; \quad \text{ACI 318-63, Section 1901 (a)}$$

$$M_a = P_a\, e_a$$

By similar triangles,

$$P_a = \frac{P_0\ M_b}{e_a\,(P_0 - P_b) + M_b} \quad \text{(Equation 5.4)}$$

b. Axial Tension and Bending

1. Concentric Tension

$$P_0 = \phi\,[A_{st}\, f_y + t_L\, f_{yL}] \quad \text{(Equation 5.5)}$$

Note: For purpose of clarity, only three steel layers were included in the preceeding equations.

5.3REINFORCING STEEL

a. Hoop, draped and elliptical steel reinforcement will be as shown on Drawing Nos. D-421-023 (Figure Drawing 2), and D-421-024 (Figure Drawing 1).

b. The amount of reinforcement which includes regular hoop steel draped around the opening and elliptical reinforcement, equals or exceeds that shown to be required by calculations. In no event is the liner assumed to contribute more than its yield strength.

c. The clear distance between parallel bars is not less than 2 times the maximum size of coarse aggregate, 2 times the bar diameter, nor less than 2 in.

d. Vertical shrinkage or temperature reinforcement is placed at outside face of wall. The minimum amount of such reinforcement on the outside concrete face wall is greater than 0.0015 of the gross cross-sectional area of concrete.

5.4MAXIMUM LINER STRESSES

The maximum liner stresses are given in Table 5-1.

5.5PENETRATION BARREL

The portions of the Equipment Access Hatch and Personnel Lock extending beyond the concrete shell were designed and fabricated by Chicago Bridge and Iron Company in accordance

with the ASME Nuclear Vessels Code. The barrel of each of these penetrations within the limit of the concrete thickness was investigated for the following loads:

a. Meridional membrane stresses in the barrel due to internal pressure on the hatch.

b. Hoop membrane stresses in the barrel due to the in-plane deformation of the opening.

c. Meridional bending stresses in the barrel caused by meridional shear transfer from the barrel to the concrete.

d. Thermal Stresses

The objective of this investigation was to verify that the stresses in the barrel are within allowable Units. Refer to ASME Nuclear Vessels Code, Article 4, Par. N-414. It should be noted that the allowable stresses referred to are based on working strength design.

5.6NORMAL SHEAR

a. Normal shears in the concrete shell surrounding the.Penetration Barrel have been computed by the Finite Element Method of analysis. The computed normal shear stress resultant, at a distance $\frac{d}{2}$ = 33.0 in. from the edge of the opening or twice the normal shear transferred by the barrel, whichever was the larger of the two, was used in the design.

b. Two modes of shear transfer are considered. First, sheer transfer through concrete without shear reinforcement. Second, disregarding the shear capacity of concrete, enough reinforcing steel is provided to carry the normal shears by steel alone.

Ultimate peripheral or normal shear stress carried by concrete is computed by:

$$v_u = \frac{Q}{d}$$

$$v_c = 4\phi (f_c')^{1/2} \quad \text{(Equation 5.6)}$$

c.

(ACI 318-63, Section 1707)

d.

where:

	Q =	normal shear stress-resultant at the critical section
	v_u =	nominal ultimate shear stress as a measure of diagonal tension
	v_c =	allowable ultimate shear stress to be carried by concrete
	d =	distance from extreme compression fiber to centroid of tension reinforcement
	f'_c =	28 days compressive strength of concrete

ϕ = 0.85

Shear reinforcement requirements

The ultimate shear capacity of the reinforcing steel alone is computed by:

$$v_u = \phi \left[A_{sv} f_y + A_{sD} \frac{f_y - f_r}{2} \right]$$ (Equation 5.7)

where:
- A_{sv} = cross-sectional area of reinforcing steel acting in tension across a potential diagonal tension crack
- A_{sD} = cross-sectional area of reinforcing steel acting in dowel action across a potential diagonal tension crack
- f_y = yield strength of reinforcement
- f_r = existing stress due to N, M in rebar also acting as a dowel
- ϕ = 0.85

5.7REBAR ANCHORAGE

a. The #18S regular hoop steel that is terminated at the penetration barrel will transfer the tensile load from the reinforcing bar to concrete by bond. As a redundancy, a mechanical anchor is provided at the end of each bar to transfer the tensile load from the reinforcing bar to the concrete in bearing. For details of anchor plates see Drawing No. D-421-024 (Figure Drawing 1).

b. Ultimate bearing stress on the concrete is computed by:

$$f_c = \frac{A_s f_y}{A_c}$$

$$F_{cu} = 0.6 f_{c_i}' \sqrt[3]{\frac{A_b'}{A_b}}$$ (Equation 5.8)

Ultimate bending stress in anchor plates will not exceed 0.90 yield strength of the anchor plate.

The transfer tensile reinforcement through the wall thickness will be determined by[33]:

$$A_{st} = \frac{\alpha A_s f_y}{0.95 f_y} = 0.105 A_s$$ (Equation 5.9)

where α = splitting force/axial force which for this design is equal to 0.1.

5.8TENDON LOSSES

The vertical post-tensioning tendons are curved around the large access openings as shown on Drawing No. D-421-023 (Figure Drawing 2).

Tendon friction losses are determined according to ACI 318-63, Chapter 26.

$$T_0 = T_x e^{(KL+\mu\alpha)}$$ (Equation 5.10)

where: K = 0.0003 (curved length only)

μ = 0.16

Tendon losses due to elastic shortening, shrinkage, creep, and steel relaxation have been determined. These losses, combined with the additional frictional losses, will require retensioning of the curved tendons after 1000 hours.

Tendon losses excluding friction after 40 years without retensioning will be approximately 16.0%.

Tendon losses excluding friction after 40 years, retensioned 1000 hours after the initial stressing, will be 11.75%.

Steel stress in any curved tendon around the large opening was determined by using the following formula:

$$T_0^{\,i}(0.8825) = T_x^{\,i} e^{(KL+\mu\alpha)}$$ (ACI 318-63 Eq. 26-2)

$$F_{s\,i} + \frac{T_x^{\,i}}{A_s}$$ (Equation 5.11)

where: f_{si} = steel stress in the i-th tendon at point x

i = i-th curved tendon

A_s area of prestressed tendons

It should be noted that the average steel stress of a group of curved tendons will be:

$$f_{s\,avg.} = \frac{\sum_{i=1}^{n} T_x^{\,i}}{N} \geq 0.6\, f_s'$$

(Equation 5.12)

where: f'_s = ultimate strength of tendon steel

N = number of curved tendons

5.9SUMMARY OF DESIGN AND CONCLUSIONS

In selecting the analytical method used for determining the stress-resultant and stress-couple distributions in the shell under all critical loading conditions an extensive bibliographic search was conducted and available methods were evaluated. In our judgment the analysis of the stresses around the openings for the R. E. Ginna Containment Vessel has been based on the most satisfactory of available methods.

The design was guided by the basic proposition that the best reinforcement is in fact the least reinforcement that will satisfy the requirement for carrying the shell loads around the opening and the normal shear applied along the opening edge into the shell out to a distance from the opening until a membrane state of stress is reached. Although not directly applicable the IITRI studies on steel containment structures conclusively showed that a stiff reinforcement around openings substantially reduces the burst strength of circular plates[34]. In our judgment this design as evidenced by the data included in Section 5 provides the required reinforcement strength and further conservatism in determining reinforcement requirements is not prudent in that the ultimate load capacity might be thereby reduced.

LIST OF REFERENCES

1. A. I. Lur′e: "Concentration of Stresses in the Vicinity of an Aperture in the Surface of a Circular Cylinder," Prikl. Mat. Mekh. 10. 1946, pp. 397-406, (English translation by N. Brunswick, N.Y. Univ., Inst. of Math. Science, 1960)

2. S. Timoshenko: "Strength of Materials, Part II," D. Van Nostrand Company, Inc., New York, N.Y., 1930, p. 457.

3. K. Sezawa and K. Kubo: "Stresses in a Plate with a Flanged Circular Hole," Report of the Aeronautical Research Institute, Tokyo Imperial University, Tokyo, Japan, No. 84, September, 1932.

4. G. Gurney: "Analysis of the Stresses in a Flat Plate with a Circular Hole Under Edge Forces," British Rep. Memo No. 1834, February, 1938.

5. Leon Beskin: "Strengthening of Circular Holes in Plates Under Edge Loads," Journal of Applied Mechanics, Trans. ASME, Vol. 66, 1944, p. A-140.

6. G. N. Savin: "Stress Concentration Around Holes," Pergamon Press, 1961.

7. D. Withum: "Die Kreiszylinderschale mit Kreisformigem Ausschnitt unter Schubbean-Spruchung," Ingerieur Archiv, XXVI, 1958, pp. 435-446.

8. V. Kline, R. C. Dixon, N. F. Jordan, and A. C. Eringen: "Stresses in Pressurized Cylindrical Shell with Cut-out," General Technology Corp. Tech. Report 3-1, 1961.

9. A. C. Eringer, A. K. Naghdi, and C. C. Thiel: "States of Stress in a Circular Cylindrical Shell with a Circular Hole," Welding Research Counci1 Bulletin 102, 1965.

10. A. K. Naghdi and A. C. Eringen: "Stress Distribution in a Circular Cylindrical Shell with a Circular Cut-out." Ingenieur Archiv.

11. J. G. Lekkerkerker "Stress Concentration Around Circular Holes in Cylindrical Shells," Eleventh Int. Congress on Applied Mechanics, Munich, 1964.

12. FELAP - Finite Element Analysis Program for Complex Structures, Franklin Institute Research Laboratories, Philadelphia, Pa.

13. Z. Zudans: "New Formulation and Evaluation of Elastic Shell Theory", Ph. D. Dissertation, University of Pennsylvania, May 1966.

14. Z. Zudans: "Analysis of Asymmetric Stiffened Shell Type Structures by the Finite Element Method," paper to be published in "Nuclear Engineering and Design."

15. J. J. Connor and C. Brebbia: "Stiffness Matrix for Shallow Rectangular Shell Elements", ASCE Journal, Vol. 93, EM5, pp. 43-65, 1967.

16. C. Prato: "A Mixed Finite-Element Method for Shell Analysis," M.I.T., June 1968.

17. M. M. Leven: "Photoelastic Determination of Stresses in Reinforced Openings in Pressure Vessels," Welding Research Council Bulletin No. 113, N.Y., 1966, pp. 25-52.

18. C. E. Taylor and N. C. Lind: "Photoelastic Study of the Stresses Near Openings in Pressure Vessels," ibid., pp. 1-24.

19. A. J. Durelli, D. J. del Rio, V. J. Parks, H. Feng: "Stresses in a Pressurized Cylinder with a Hole," Journal ASCE, Vol. 93, ST5, 1967, pp. 383-399.

20. R. Mark and J. D. Riera: Discussion of Ref. (19), Journal ASCE, Vol. 94, ST4, pp. 1075-76.

21. D. S. Houghton and A. Rothwell: "The Influence of Curvature on the State of Stress Ahead of Cracks in Cylindrical Shells." Non-Classical Shell Problems, Proc. of the Int. Symposium on Non-Classical Shell Problems, Warsaw, Poland, 1963, North Holland, 1964, pp. 685-700.

22. S. K. Takahashi and R. Mark: "Analysis and Photoelastic Investigations of Stress Concentrations in Sphere-Cylinder Configurations," U. S. Naval Civil Engineering Laboratory Report.

23. J. H. Barnwell and C. H. Edwards: "The Development and Testing of Three-Dimensional Photoelastic Models of Pretensioned, Prestressed Concrete Beams," paper presented at the 1968 SESA Spring Meeting, May 1968, Albany, N.Y.

24. R. Mark: "Photomechanical Model Analysis of Concrete Structures," ACI Symposium on Models, 1968.

25. J. L. Mershon: "Preliminary Evaluation of PVRC Photoelastic Test Data on Reinforced Openings in Pressure Vessels," Welding Research Council Bulletin No. 113, 1966.

26. G. N. Savin: "Concentration of Stresses around Curvilinear Holes in Plates and Shells," Eleventh International Congress of Applied Mechanics, Munich, 1964.

27. Ch. H. Lerchenthal: "A Photoelastic Investigation of Stress Concentration Around Reinforced Cut-outs in Stresses Sheets," ibid.

28. I. E. Milekykovsky: "Some Problems of Analysis of Reinforced Concrete Cylindrical Shell Roofs Taking into Consideration Crack Formation," Non-Classical Shell Problems, Proc. of the Symposium on Non-Classical Shell Problems, Warsaw, Poland, 1963, North Holland 1964, p. 1152.

29. A. W. Hedgran and D. P. Billington: "Mortar Model Test on a Cylindrical Shell of Varying Curvature and Thickness," ACI Journal, V. 64, 1967, p. 73-83.

30. J. D. Riera and D. P. Billington: "Non-Linear Analysis of Reinforced Concrete Thin Shell Roofs," Dept. of Civil and Geological Engineering, Research Report, Princeton University, Princeton, New Jersey, (in preparation).

31. Y. R. Rashid: "Analysis of Axisymmetric Composite Structures by the Finite Element Method," Nuclear Engineering and Design 3 (1666) 163-182, North-Holland Publishing Company, Amsterdam.

32. O. C. Zienkiewicz and Y. K. Cheung, "The Finite Element Method in Structural and Continum Mechanics," McGraw-Hill Publishing Company Ltd. (1967 Edition).

33. F. Leonhardt: "Prestressed Concrete Design and Construction," Wilhelm Ernst & Sohn, Berlin, 1964.

34. M. A. Salmon: "Studies of Reactor Containment Structures," IITRI Final Report for U.S. AEC, Dept. of Commerce, Washington, D.C., 1966.

35. F. Yao "Finite-Element Method for Shell Analysis," Ph.D. Dissertation, M.I.T. January 1968.

Table 4-1
Load Combinations

LOAD COMBINATIONS			FUNDAMENTAL LOADS							
			DL(1)	VP(2)	OT(3)	AT(4)	IP(5)	Bo(6)	E1(7)	E2(8)
	Normal* Operation	1	1.0	1.17	0.4					
		2	1.0	1.0	0.4					
		3	1.0	1.17	1.0					
		4	1.0	1.0	1.0					
	Test Pressure	5	1.0	1.17	0.4		1.0			
		6	1.0	1.0	0.4		1.0			
		7	1.0	1.17	0.4		1.0	1.0		
		8	1.0	1.0	0.4		1.0	1.0		
		9	1.0	1.17	1.0		1.0			
		10	1.0	1.0	1.0		1.0			
		11	1.0	1.17	1.0		1.0	1.0		
		12	1.0	1.0	1.0		1.0	1.0		
	Accident Pressure Loadings	13	1.0	1.17	1.0	1.0	1.304			
		14	1.0	1.0	1.0	1.0	1.304			
		15	1.0	1.17	0.4	1.0	1.304			
		16	1.0	1.0	0.4	1.0	1.304			
		17	1.0	1.17	1.0	1.0	1.304	1.304		
		18	1.0	1.0	1.0	1.0	1.304	1.304		
		19	1.0	1.17	0.4	1.0	1.304	1.304		
		20	1.0	1.0	0.4	1.0	1.304	1.304		
		21	1.0	1.17	1.0	0.92	1.087			0.404
		22	1.0	1.0	1.0	0.92	1.087			0.404
		23	1.0	1.17	0.4	0.92	1.087			0.404
		24	1.0	1.0	0.4	0.92	1.087			0.404
		25	1.0	1.17	1.0	0.92	1.087	1.087		0.404
		26	1.0	1.0	1.0	0.92	1.087	1.087		0.404
		27	1.0	1.17	0.4	0.92	1.087	1.087		0.404
		28	1.0	1.0	0.4	0.92	1.087	1.087		0.404
		29	1.0	1.17	1.0	0.92	1.087		0.404	
		30	1.0	1.0	1.0	0.92	1.087		0.404	
		31	1.0	1.17	0.4	0.92	1.087		0.404	
		32	1.0	1.0	0.4	0.92	1.087		0.404	
		33	1.0	1.17	1.0	0.92	1.087	1.087	0.404	
		34	1.0	1.0	1.0	0.92	1.087	1.087	0.404	
		35	1.0	1.17	0.4	0.92	1.087	1.087	0.404	
		36	1.0	1.0	0.4	0.92	1.087	1.087	0.404	
		37	1.0	1.17	1.0	0.92	1.087		-0.404	
		38	1.0	1.0	1.0	0.92	1.087		-0.404	
		39	1.0	1.17	0.4	0.92	1.087		-0.404	
		40	1.0	1.0	0.4	0.92	1.087		-0.404	
		41	1.0	1.17	1.0	0.92	1.087	1.087	-0.404	
		42	1.0	1.0	1.0	0.92	1.087	1.087	-0.404	
		43	1.0	1.17	0.4	0.92	1.087	1.087	-0.404	
		44	1.0	1.0	0.4	0.92	1.087	1.087	-0.404	
		45	1.0	1.17	1.0	0.92	1.087			-0.404
		46	1.0	1.0	1.0	0.92	1.087			-0.404
		47	1.0	1.17	0.4	0.92	1.087			-0.404
		48	1.0	1.0	0.4	0.92	1.087			-0.404
		49	1.0	1.17	1.0	0.92	1.087	1.087		-0.404
		50	1.0	1.0	1.0	0.92	1.087	1.087		-0.404
		51	1.0	1.17	0.4	0.92	1.087	1.087		-0.404
		52	1.0	1.0	0.4	0.92	1.087	1.087		-0.404
		53	1.0	1.17	1.0	0.85	0.87		1.0	
		54	1.0	1.0	1.0	0.85	0.87		1.0	
		55	1.0	1.17	0.4	0.85	0.87		1.0	
		56	1.0	1.0	0.4	0.85	0.87		1.0	
		57	1.0	1.17	1.0	0.85	0.87	0.87	1.0	
		58	1.0	1.0	1.0	0.85	0.87	0.87	1.0	
		59	1.0	1.17	0.4	0.85	0.87	0.87	1.0	
		60	1.0	1.0	0.4	0.85	0.87	0.87	1.0	
		61	1.0	1.17	1.0	0.85	0.87		-1.0	
		62	1.0	1.0	1.0	0.85	0.87		-1.0	
		63	1.0	1.17	0.4	0.85	0.87		-1.0	
		64	1.0	1.0	0.4	0.85	0.87		-1.0	
		65	1.0	1.17	1.0	0.85	0.87	0.87	-1.0	
		66	1.0	1.0	1.0	0.85	0.87	0.87	-1.0	
		67	1.0	1.17	0.4	0.85	0.87	0.87	-1.0	
		68	1.0	1.0	0.4	0.85	0.87	0.87	-1.0	
		69	1.0	1.17	1.0	0.85	0.87			-1.0
		70	1.0	1.0	1.0	0.85	0.87			-1.0
		71	1.0	1.17	0.4	0.85	0.87			-1.0
		72	1.0	1.0	0.4	0.85	0.87			-1.0
		73	1.0	1.17	1.0	0.85	0.87	0.87		-1.0
		74	1.0	1.0	1.0	0.85	0.87	0.87		-1.0
		75	1.0	1.17	0.4	0.85	0.87	0.87		-1.0
		76	1.0	1.0	0.4	0.85	0.87	0.87		-1.0

DL = Dead Load
VP = Vertical Prestress
OT = Operating Temp.
AT = Accident Temp.
IP = Internal Pressure
B_o = Loss of Bond
E_1 = Earthquake 1
E_2 = Earthquake 2

Note: Coefficients are based on: Test pressure
Winter temp.
Final Prestress
Max. Hypothetical Earthquake

*Distributions for normal operation based on uncracked model.

Initial prestress: $\frac{.7}{.6} = \underline{\underline{1.17}}$

Pressure Load:

$\frac{1.5}{1.15} = 1.3043$ $\quad \frac{1.25}{1.15} = 1.0870$ $\quad \frac{1.0}{1.15} = 0.8696$

Earthquake: 0.2g - 2% damp → 0.47 $\quad r = \frac{0.19}{0.47} = 0.404$
0.08g 2% damp → 0.19

Accident temp: 90 psig 1.5p→ T = 312°F r = 1.0
75 psig 1.25p→T = 285°F r = 285/312 = 0.92
60 psig 1.0p→ T = 265°F r = 265/312 = 0.85

GILBERT ASSOCIATES, IN

Table 4-2
Stress Around Equipment Hatch-Loading (Uncracked Shell)

STRESS AROUND EQUIPMENT HATCH
LOADING CONDITION NO. 2
Vertical Prestress (Final)

	Axial Direction		Hoop Direction		Membrane Shear	Normal	Shears
	N_ϕ	M_ϕ	N_θ	M_θ	$N_{\phi\theta}$	Q_ϕ	Q_θ
11	-22.410	- 18.050	1.428	- 3.797	0.166	1.101	0.001
22	-19.470	- 72.220	2.573	23.639	1.065	0.418	0.039
33	-15.232	- 87.135	2.975	75.887	1.382	-0.900	0.184
44	-10.148	- 63.587	3.005	95.206	2.070	-1.271	0.297
55	- 5.290	- 22.978	4.664	122.587	2.243	-0.227	-0.219
66	- 2.056	1.545	8.666	170.009	2.252	0.316	-0.841
77	0.064	31.434	17.139	273.855	.384	5.411	0.324
25	-32.907	-212.489	4.786	61.086	0.355	2.654	-0.844
49	-34.615	-307.571	6.387	78.725	2.061	1.699	-0.930
73	-38.819	-377.591	4.024	63.011	4.300	0.585	-1.245
74	-31.907	-308.348	-2.301	79.870	7.999	-0.190	3.254
94	-23.312	31.380	3.933	- 42.611	-0.127	-0.006	-0.551
97	-38.051	-405.931	1.403	- 5.139	-0.077	0.073	0.345
99	-43.620	33.491	-3.261	421.929	0.409	0.366	0.962
100	-52.537	-478.211	-6.196	- 48.723	1.671	1.480	0.738
101	-62.902	-612.005	-6.349	- 60.802	3.436	-3.406	-7.782

Note: N_ϕ, N_θ, $N_{\phi\theta}$, Q_ϕ and Q_θ in Kips/in. M_ϕ and M_θ in Kips.

Values computed by finite-element analysis of uncracked shell.

Sheet 1 of 2

GILBERT ASSOCIATES, INC.

STRESS AROUND EQUIPMENT HATCH
LOADING CONDITION NO. 4
69 psi Internal Pressure

	Axial Direction		Hoop Direction		Membrane Shear	Normal	Shears
	N_ϕ	M_ϕ	N_θ	M_θ	$N_{\phi\theta}$	Q_ϕ	Q_θ
11	22.350	138.494	43.708	14.810	- 0.028	1.438	0.009
22	22.208	74.061	49.821	230.145	- 0.004	0.895	-0.035
33	21.764	40.226	63.614	582.624	- 0.339	- 0.063	-0.135
44	19.749	43.602	67.554	602.660	- 1.021	- 0.740	-0.084
55	16.294	82.115	75.487	651.797	- 2.272	5.219	-1.298
66	12.291	107.555	86.917	746.735	- 4.078	8.460	-2.052
77	4.827	129.865	100.974	942.268	6.999	18.022	5.028
25	24.344	48.384	49.209	273.717	- 1.193	- 0.974	-2.980
49	25.229	86.106	45.915	347.055	- 8.114	- 2.250	-2.614
73	28.609	178.390	36.473	332.698	-17.349	- 4.008	-0.998
74	26.820	64.056	38.803	351.177	-24.430	-13.956	-3.537
94	20.988	- 21.114	35.201	63.859	- 0.342	- 0.032	-1.770
97	35.276	374.791	26.405	164.953	- 1.747	- 0.706	0.393
99	37.272	385.443	15.239	131.236	- 3.218	- 0.984	1.455
100	38.959	388.064	7.885	106.644	- 4.163	- 1.473	2.016
101	36.600	404.216	0.533	73.195	- 3.367	3.706	6.202

Note: N_ϕ, N_θ, $N_{\phi\theta}$, Q_ϕ and Q_θ in Kips/in. M_ϕ and M_θ in Kips.

Values computed by finite-element analysis of uncracked shell.

Sheet 2 of 2

GILBERT ASSOCIATES, INC.

Table 4-3
Stress Around Equipment Hatch-Loading (Cracked Shell)

STRESS AROUND EQUIPMENT HATCH
LOADING CONDITION NO. 1
Dead Load

	Axial Direction		Hoop Direction		Membrane Shear	Normal	Shears	Twisting Moment
	N_ϕ	M_ϕ	N_θ	M_θ	$N_{\phi\theta}$	Q_ϕ	Q_θ	$M_{\phi\theta}$
11	- 2.09	- 11.58	-0.06	0.01	0.07	0.02	0.	-0.09
22	- 1.86	- 13.95	-0.17	-0.01	0.10	0.03	-0.04	0.71
33	- 1.24	- 3.30	-0.17	-1.73	0.15	-0.24	0.03	1.52
44	- 0.72	1.74	0.23	1.36	0.20	-0.22	0.02	1.55
55	- 0.27	3.16	0.66	4.85	0.19	0.01	-0.03	0.66
66	0.	2.58	1.14	8.91	0.18	0.11	-0.09	0.46
77	0.16	0.56	2.05	16.35	-0.10	0.51	-0.17	-1.90
25	- 5.00	- 32.56	0.15	3.58	-0.11	0.21	-0.10	-7.68
49	- 5.19	- 40.21	0.23	4.04	-0.16	0.25	-0.05	-5.60
73	- 6.53	- 63.65	0.23	5.70	-0.02	0.32	0.14	-7.29
74	- 4.49	- 29.16	0.14	0.91	0.63	-0.15	0.12	-3.22
94	- 3.49	4.93	0.12	-3.94	-0.01	0.	-0.16	-0.06
97	- 4.96	- 40.64	-0.32	3.10	-0.06	0.01	-0.02	-1.01
99	- 5.82	- 46.02	-0.62	2.36	-0.13	-0.07	0.05	-2.17
100	- 7.40	- 59.79	-0.87	1.11	-0.16	0.33	0.20	-2.67
101	-11.74	-102.48	-0.86	2.91	0.66	1.35	0,27	3.58

Note: N_ϕ, N_θ, $N_{\phi\theta}$, Q_ϕ and Q_θ in Kips/in. M_ϕ, M_θ, and $M_{\phi\theta}$ in Kips.
Values computed by finite-element analysis of cracked shell.

Sheet 1 of 8

GILBERT ASSOCIATES, INC.

STRESS AROUND EQUIPMENT HATCH
LOADING CONDITION NO. 2
Vertical Prestress (FINAL)

	Axial Direction		Hoop Direction		Membrane Shear	Normal	Shears	Twisting Moment
	N_ϕ	M_ϕ	N_θ	M_θ	$N_{\phi\theta}$	Q_ϕ	Q_θ	$M_{\phi\theta}$
11	-18.19	-105.15	1.66	1.57	-0.08	0.26	-0.0	0.50
22	-16.72	-128.36	1.70	4.67	1.14	0.48	-0.27	3.36
33	-11.49	- 54.12	1.29	17.71	1.21	-1.75	0.14	10.10
44	- 7.34	- 12.24	0.64	13.36	1.48	-1.74	0.14	9.32
55	- 4.09	2.50	0.98	18.31	1.39	-0.67	0.09	3.26
66	- 2.10	- 5.56	2.14	29.98	1.55	0.03	-0.68	3.01
77	- 0.51	- 14.23	5.59	59.5	0.24	1.61	-1.28	- 6.66
25	-31.80	-207.2	1.40	19.38	0.39	1.57	-0.49	-39.14
49	-32.93	-258.52	2.07	16.50	1.60	1.82	-0.33	-22.81
73	-40.68	-389.59	2.44	34.18	3.97	0.38	0.84	-25.94
74	-29.51	-172.09	-3.03	- 8.08	6.09	-0.91	1.0	-21.27
94	-22.78	29.11	3.26	-15.84	0.05	0.02	-0.56	- 0.22
97	-35.03	-322.31	2.50	10.80	0.20	0.28	-0.21	- 1.75
99	-39.93	-311.45	-0.33	4.15	0.60	-0.52	-0.53	- 1.67
100	-48.64	-352.39	-3.76	8.52	0.83	1.95	-0.05	- 2.73
101	-69.91	-529.52	-5 85	22.70	5.28	5.88	-1.11	22.15

Note: N_ϕ, N_θ, $N_{\phi\theta}$, Q_ϕ and Q_θ in Kips/in. M_ϕ, M_θ, and $M_{\phi\theta}$ in Kips.

Values computed by finite-element analysis of cracked shell.

Sheet 2 of 8

GILBERT ASSOCIATES, INC.

STRESS AROUND EQUIPMENT HATCH
LOADING CONDITION NO. 3
Operating Temperature (WINTER)

	Axial Direction		Hoop Direction		Membrane Shear	Normal	Shears	Twisting Moment
	N_ϕ	M_ϕ	N_θ	M_θ	$N_{\phi\theta}$	Q_ϕ	Q_θ	$M_{\phi\theta}$
11	- 8.70	123.86	1.73	51.13	- .01	-1.49	0.02	- 0.36
22	- 8.12	180.47	- .80	50.39	.18	-1.69	.09	- 3.02
33	- 7.54	197.31	- 1.01	85.14	.31	-1.57	0.06	- 7.46
44	- 6.35	190.36	- 8.21	37.54	0.55	-1.45	0.04	-11.47
55	- 4.86	167.34	-13.01	9.12	0.89	-1.08	-0.40	-11.14
66	- 2.75	172.01	-19.78	- 35.85	1.20	1.23	2.60	-20.60
77	- 0.20	128.64	-32.56	-123.57	2.67	-2.87	3.75	-23.16
25	- 3.78	363.61	- 3.82	36.28	-3.50	-2.56	0.21	-44.20
49	- 5.61	454.02	- 3.94	39.53	-4.51	-1.65	-0.32	-92.31
73	-24.92	357.52	- 8.59	- 1.10	0.79	2.37	0.13	-80.09
74	-30.11	-233.75	-13.83	- 45.07	9.72	0.08	-0.48	-74.01
94	5.45	162.68	- 2.75	33.64	-0.07	0.03	-0.53	- 0.80
97	- 2.17	622.03	- 3.68	27.20	-0.26	-0.69	-0.86	- 8.25
99	-18.67	540.17	- 5.02	34.79	-0.36	-0.32	-2.04	-22.36
100	-38.57	422.50	- 5.27	37.52	0.30	0.95	-2.95	-24.41
101	-80.37	94.07	- 2.78	25.19	5.77	3.53	4.62	-24.39

Note: N_ϕ, N_θ, $N_{\phi\theta}$, Q_ϕ and Q_θ in Kips/in. M_ϕ, M_θ, and $M_{\phi\theta}$ in Kips.
Values computed by finite-element analysis of cracked shell.

Sheet 3 of 8

GILBERT ASSOCIATES, INC.

STRESS AROUND EQUIPMENT HATCH
LOADING CONDITION NO. 4
Accident Temperature

	Axial Direction		Hoop Direction		Membrane Shear	Normal	Shears	Twisting Moment
	N_ϕ	M_ϕ	N_θ	M_θ	$N_{\phi\theta}$	Q_ϕ	Q_θ	$M_{\phi\theta}$
11	-1.45	-13.56	.76	1.57	- .06	.15	- .01	0.25
22	-1.73	8.88	.94	1.21	-0.11	.12	- .09	0.05
33	-2.11	7.21	2.55	20.71	- .16	.05	- .10	- 0.86
44	-2.86	8.72	3.38	27.85	- .34	- .18	- .14	- 3.27
55	-3.65	10.24	4.80	37.39	- .53	-0.05	-0.40	- 6.38
66	-4.60	15.51	6.02	49.72	- .82	0.11	-0.30	- 8.04
77	-5.84	15.94	7.93	68.66	-1.28	1.95	0.47	-13.56
25	.09	3.95	.29	1.76	- .55	- .16	- .05	- 2.29
49	.21	8.12	.05	3.71	-1.43	- .06	- .13	- 2.22
73	1.27	11.80	- .70	- .10	-3.00	.64	.03	- 2.24
74	.14	24.26	- .43	-10.75	-4.81	-2.02	- .36	- 5.93
94	.49	- .28	- .51	- 2.76	- .03	0.	- .18	- .02
97	1.91	15.73	-1.37	3.63	- .20	- .08	.17	- .54
99	3.06	- 2.51	-2.48	5.98	- .36	.13	.66	1.20
100	4.78	-24.63	-3.56	4.04	- .90	0.43	1.61	4.07
101	5.53	-71.13	-5.03	- 5.38	-2.09	-0.88	3.53	6.61

Note: N_ϕ, N_θ, $N_{\phi\theta}$, Q_ϕ and Q_θ in Kips/in. M_ϕ, M_θ, and $M_{\phi\theta}$ in Kips.

Values computed by finite-element analysis of cracked shell.

Sheet 4 of 8

GILBERT ASSOCIATES, INC.

STRESS AROUND EQUIPMENT HATCH
LOADING CONDITION NO. 5
69 psi Internal Pressure

	Axial Direction		Hoop Direction		Membrane Shear	Normal	Shears	Twisting Moment
	N_ϕ	M_ϕ	N_θ	M_θ	$N_{\phi\theta}$	Q_ϕ	Q_θ	$M_{\phi\theta}$
11	20.02	264.15	39.59	22.93	0.52	6.21	- 0.20	5.63
22	25.52	96.70	34.32	- 12.86	1.34	3.30	- 1.00	15.99
33	27.82	10.82	69.99	481.80	0.33	1.96	- 1.08	22.40
44	26.42	30.86	76.32	517.73	- 1.13	- 0.33	- 0.64	11.04
55	22.91	50.91	87.83	596.92	- 2.14	5.20	- 3.33	1.93
66	20.79	154.48	100.23	685.26	- 3.81	6.34	- 0.69	- 1.64
77	14.63	170.28	121.52	848.44	-11.12	19.25	1.79	- 73.84
25	24.54	94.49	44.14	33.84	0.29	- 2.69	0.43	100.47
49	20.91	33.51	42.34	46.48	- 4.90	3.68	- 4.76	22.94
73	25.42	8.15	48.55	396.22	-22.52	2.75	- 1.95	-157.81
74	29.33	43.58	53.02	567.11	-28.25	-15.01	- 2.21	-154.40
94	20.53	- 86.57	42 07	19.85	- 0.05	0.05	- 0.66	- 0.37
97	35.56	223.25	29.19	- 29.24	- 2.29	- 3.11	1.61	- 16.85
99	41.39	193.13	15.10	4.38	- 3.36	- 1.31	1.11	- 17.92
100	45.71	182.31	8.48	7.61	- 4.57	- 1.98	2.81	- 32.13
101	39.72	59.79	0.04	2.66	- 5.25	4.79	11.59	- 19.30

Note: N_ϕ, N_θ, $N_{\phi\theta}$, Q_ϕ and Q_θ in Kips/in. M_ϕ, M_θ, and $M_{\phi\theta}$ in Kips.
Values computed by finite-element analysis of cracked shell.

Sheet 5 of 8

GILBERT ASSOCIATES, INC.

STRESS AROUND EQUIPMENT HATCH
LOADING CONDITION NO. 6
Effect of Bond Loss Associated With 69 psi

	Axial Direction		Hoop Direction		Membrane Shear	Normal	Shears	Twisting Moment
	N_ϕ	M_ϕ	N_θ	M_θ	$N_{\phi\theta}$	Q_ϕ	Q_θ	$M_{\phi\theta}$
11	3.92	62.18	- 0.25	0.91	0.04	0.69	- 0.03	0.56
22	4.34	51.42	- 0.21	- 3.85	- 0.01	0.09	- 0.09	2.61
33	3.99	42.07	- 0.56	-17.27	- 0.05	0.46	0.	3.22
44	3.69	39.12	0.44	-12.62	- 0.19	0.52	- 0.14	1.56
55	3.08	36.96	1.67	- 5.30	- 0.39	0.69	- 0.45	2.02
66	2.69	51.66	3.12	4.48	- 0.77	0.65	0.62	- 1.10
77	1.85	48.44	4.19	12.59	- 0.79	0.78	1.45	- 6.88
25	- 1.02	14.36	- 0.69	- 6.02	- 1.02	0.77	0.09	2.82
49	- 4.21	- 55.67	- 1.94	8.79	- 1.39	0.79	0.13	- 7.98
73	- 6.74	-111.31	- 5.27	- 3.53	- 3.62	- 1.24	- 1.55	9.91
74	7.24	67.19	0.38	-15.12	- 1.29	2.25	- 3.59	53.00
94	- 1.97	- 10.08	3.83	34.02	0.13	- 0.97	1.39	0.44
97	7.09	- 0.94	-13.70	- 0.87	6.16	- 0.31	- 0.72	65.16
99	14.07	164.57	-29.94	19.74	0.97	- 1.18	0.44	3.32
100	11.03	82.57	-45.63	26.25	-15.91	-21.56	4.62	-150.49
101	-25.20	-602.32	15.18	12.79	-30.42	44.29	23.33	-126.64

Note: N_ϕ, N_θ, $N_{\phi\theta}$, Q_ϕ and Q_θ in Kips/in. M_ϕ, M_θ, and $M_{\phi\theta}$ in Kips.
Values computed by finite-element analysis of cracked shell.

Sheet 6 of 8

GINNA/UFSAR
TABLE 4.3

46

STRESS AROUND EQUIPMENT HATCH
LOADING CONDITION NO. 7
Earthquake #1

	Axial Direction		Hoop Direction		Membrane Shear	Normal	Shears	Twisting Moment
	N_ϕ	M_ϕ	N_θ	M_θ	$N_{\phi\theta}$	Q_ϕ	Q_θ	$M_{\phi\theta}$
11	- 3.80	- 21.08	- .109	.018	0.127	0.036	0.	- 0.18
22	- 3.39	- 25.39	-0.309	- 0.018	0.182	0.055	-0.073	1.36
33	- 2.26	- 6.01	-0.309	- 3.15	0.273	-0.437	0.055	2.90
44	- 1.31	3.17	0.419	2.48	0.364	-0.400	0.036	2.98
55	- 0.491	5.75	1.20	8.83	0.346	0.018	-0.055	1.27
66	0.	4.70	2.07	16.22	0.328	0.200	-0.164	0.88
77	0.291	1.02	3.73	29.76	-0.182	0.928	-0.309	- 3.65
25	- 9.10	- 59.26	0.273	6.52	-0.200	0.382	-0.182	-14.70
49	- 9.45	- 73.18	0.419	7.35	-0.291	0.455	-0.091	-10.70
73	-11.88	-115.84	0.419	10.37	-0.036	0.582	0.255	-14.00
74	- 8.17	- 53.07	0.255	1.66	1.15	-0.273	0.218	- 6.17
94	- 6.35	8.97	0.218	- 7.17	-0.018	0.	-0.291	- 0.12
97	- 9.03	- 73.96	-0.582	5.64	-0.109	0.018	-0.036	- 1.93
99	-10.59	- 83.76	-1.13	4.30	-0.237	-0.127	0.091	- 4.18
100	-13.47	-108.81	-1.58	2.02	-0.291	0.601	0.364	- 5.14
101	-21.37	-186.51	-1.57	5.30	1.20	2.46	0.491	6.85

Note: N_ϕ, N_θ, $N_{\phi\theta}$, Q_ϕ and Q_θ in Kips/in. M_ϕ, M_θ, and $M_{\phi\theta}$ in Kips.

Sheet 7 of 8

TABLE 4.2

STRESS AROUND EQUIPMENT HATCH
LOADING CONDITION NO. 8
Earthquake #2

	Axial Direction		Hoop Direction		Membrane Shear	Normal	Shears	Twisting Moment
	N_ϕ	M_ϕ	N_θ	M_θ	$N_{\phi\theta}$	Q_ϕ	Q_θ	$M_{\phi\theta}$
11	- 0.49	- 2.52	0.	0.	5.0			
22	- 0.43	- 3.26	- 0.04	0.	5.0			
33	- 0.28	- 0.77	- 0.04	-0.4	4.0			
44	- 0.17	0.41	0.05	0.3	3.0			
55	- 0.06	0.74	0.2	1.1	2.0			
66	0.	0.61	0.3	2.1	1.0			
77	0.	0.14	0.5	3.8	0.			
25	- 1.2	- 7.6	0.	0.8	0.	NEGLIGIBLE	NEGLIGIBLE	NEGLIBIBLE
49	- 4.2	- 9.2	- 3.	1.	3.0			
73	- 6.5	-14.8	- 6.	1.3	6.0			
74	-11.7	- 6.8	-10.6	0.2	10.9			
94	- 0.8	1.1	0.	-0.9	5.			
97	- 1.16	- 9.4	- 0.1	0.7	4.			
99	- 1.37	-10.8	- 0.2	0.5	3.			
100	- 1.73	-14.	- 0.2	0.2	2.			
101	- 2.74	-24.	- 0.2	0.7	0.			

Note: N_ϕ, N_θ, $N_{\phi\theta}$, Q_ϕ and Q_θ in Kips/in. M_ϕ, M_θ, and $M_{\phi\theta}$ in Kips.

Sheet 8 of 8

GILBERT ASSOCIATES, INC.

Table 5-1
Maximum Liner Stresses Stress tangent to the edge in Ksi

		σ_t	
Element	**Load#**	***[1]***	***[2]***
77	19	+34*	+55*
74	20	+25	+36*
101	25	-23	-7

Note:

[1] Composite action neglected

[2] Composite action included

* As a measure of strain

APPENDIX A TO APPENDIX 3B

EFFECT OF CONCRETE CREEP AND THE SUSTAINED OPERATING STRESSES ON STRESS DISTRIBUTION AROUND OPENINGS IN A RAPIDLY PRESSURIZED REINFORCED CONCRETE VESSEL

3B.A EFFECT OF CONCRETE CREEP AND THE SUSTAINED OPERATING STRESSES ON STRESS DISTRIBUTION AROUND OPENINGS IN A RAPIDLY PRESSURIZED REINFORCED CONCRETE VESSEL

Consider the simple structure shown below:

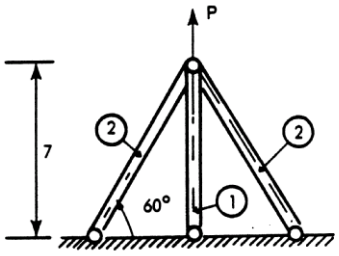

Figure A-1

Column (1) is a reinforced concrete column with net concrete area A_c^1 and longitudinal steel Area A_{st}^1 . A_c^2 and A_{st}^2 denote the net concrete area and the longitudinal steel area, respectively, of reinforced concrete columns (2). The system is loaded at time t = 0 with a vertical load P. Let us determine the initial load distribution:

$$P = T_1 + 2T_2 \sin 60° = T_1 + \sqrt{3}\ T_2 \qquad \text{(Equation 1)}$$

$$\Delta L_2 = \Delta L_1 \sin 60°; \quad \Delta L_2 = \frac{\sqrt{3}}{2}\ \Delta L_1 \qquad \text{(Equation 2)}$$

in which $$\frac{\Delta L_1}{L} = \frac{T_1}{A_c^1 E_c + A_{st} E_{st}^1} \qquad \text{(Equation 3)}$$

$$\frac{\sqrt{3}}{2}\ \frac{\Delta L_2}{L} = \frac{T_2}{A_c^2 E_c + A_{st}^2 E_{st}} \qquad \text{(Equation 4)}$$

E_c and E_{st} denote the "effective" modules of elasticity of concrete and steel, T_1 and T_2 the loads carried by columns (1) and (2), respectively. From equations (1) to (4) we obtain:

$$T_1 + \sqrt{3}\ T_2 = P$$

$$\frac{\sqrt{3}}{2}\frac{\Delta L\, T_1}{A_c^1 E_c + A_{st}^1 E_{st}} - \frac{2}{\sqrt{3}}\frac{L\, T_2}{A_c^2 E_c + A_{st}^2 E_{st}} = 0$$

or $$\begin{Bmatrix} T_1 \\ T_2 \end{Bmatrix} = \begin{Bmatrix} \frac{\beta}{1.5\alpha+\beta} \\ \frac{\sqrt{3}}{2}\frac{\alpha}{1.5\alpha+\beta} \end{Bmatrix} P$$ (Equation 5)

In which

$$\alpha = \frac{L}{A_c^1 E_c + A_{st}^1 E_{st}}$$

$$\beta = \frac{2}{\sqrt{3}}\frac{L}{A_c^2 E_c + A_{st}^2 E_{st}}$$ (Equation 6)

Equation (5) gives the loads acting on columns (1) and (2) in terms of the "effective" modulae E_c and E_{st}.

In general, T_1 and T_2 will change with time (load redistribution) due to concrete creep. Under the assumption that concrete behaves like a Kelvin-type material, the load distribution may be calculated exactly for $t \rightarrow \infty$ by resorting to the creep-limit modulus E_{cu}. (Time-dependent behavior of steel is neglected.)

Note that even when there is no load redistribution (for example, when $\alpha = \beta$) there will be some stress redistribution. In other words, T_1 and T_2 may remain constant, but the percentage of both carried by the steel reinforcement will increase as concrete creeps. As a result, steel stresses will increase and concrete stresses will decrease to final values which may be easily computed.

Let us now assume that at time t_1 a load P_1 is superimposed on the existing load P_0 giving a total load $(P_0 + P_1)$. (See Figure A-1). Let T_1 and T_2 be the column loads immediately before the load P_1 is applied. To compute the actual column loads T_1 and T_2 after P_1 is applied, we would be tempted to determine the column loads T_1^* and T_2^* corresponding to P_1 acting alone on the structure (On the basis of the initial modulus of elasticity) and then add them to T_1^1 and T_2^1:

$$T_1^2 = T_1^1 + T_1^*$$ (Equation 7)

$$T_2^2 = T_2^1 + T_2^* \quad \text{(Equation 8)}$$

The approach is valid if there is no concrete cracking. If either column (1) or (2) (or both) cracks due to the resluting tensile stresses, the results obtained by resorting to equation (7) will be incorrect. The situation will be best illustrated by an example. Let:

E_c^0 = initial modulus of elasticity of concrete = 4000 ksi

E_c^u = "final" effective modulus of elasticity of concrete = 2000 ksi

E_{st} = $7.5\ E_c^0$ = 3000 ksi

A_c^1 = 100 in.^{2}

A_c^2 = 100 in.^{2}

A_{st}^1 = 2 in.^{2}

A_{st}^2 = 4 in.^{2}

L = 1000 in.

A load P_0 = -200 kips is applied at t = 0 and kept constant.

At time $t = t_1$ a second load P_1 = +300 kips is applied.

Initial Load Distribution under $P = P_0$

$$\alpha_i = \frac{1000}{100 + 2 \times 7.5} \frac{1}{E_c^0} = \frac{8.69}{E_c^0} \quad \text{(Equation 9)}$$

$$\beta_i = \frac{2}{\sqrt{3}} \frac{1000}{100 + 4 \times 7.5} \frac{1}{E_c^0} = \frac{8.875}{E_c^0} \quad \text{(Equation 10)}$$

$$T_1^0 = \frac{8.875}{1.5 \times 8.69 + 8.875} P_0 = 0.404 P_0$$

$$T_2^0 = \frac{8.69 \times 0.866}{1.5 \times 8.69 + 8.875} P_0 = 0.343 P_0 \quad \text{(Equation 11)}$$

Load Distribution under P = P_0 Immediately Before Application of P_1 ($t_1 \rightarrow \infty$)

$$\alpha_f = \frac{1000}{0.5 \times 100 + 2 \times 7.5} \frac{1}{E_c^{\,0}} = \frac{15.4}{E_c^{\,0}}$$

$$\beta_f = \frac{1.155 \times 1000}{0.5 \times 100 + 4 \times 7.5} \frac{1}{E_c^{\,0}} = \frac{14.45}{E_c^{\,0}} \quad \text{(Equation 12)}$$

$$T_{11}^{1} = \frac{14.45}{1.5 \times 15.4 + 14.45} P_0 = 0.385 P$$

$$T_2^{1} = \frac{15.4 \times 0.866}{1.5 \times 15.4 + 14.45} P_0 = 0.355 P_0 \quad \text{(Equation 13)}$$

Concrete Stresses Due to P = P_0

Initial Stresses

$$\begin{cases} f_{c_1}^{\,0} = \dfrac{\alpha_i T_1 E_c^{\,0}}{L} = -704 \ psi \\ f_{c_1}^{\,0} = \dfrac{\beta_i T_2 E_c^{\,0}}{L} = -608 \ psi \end{cases} \quad \text{(Equation 14)}$$

Final Stresses ($t_1 \rightarrow \infty$)

$$\begin{cases} f_{c_1}^{-1} = \dfrac{\alpha_f T_1 E_c^{\,u}}{L} = -598 \ psi \\ f_{c_2}^{-1} = \dfrac{\beta_f T_2 E_c^{\,u}}{L} = -514 \ psi \end{cases} \quad \text{(Equation 15)}$$

Consequently, if t_1 is large, concrete stresses immediately after P_1 is applied would be:

$$f_{c_1}^{1+} = -598 + 1055 = +457 \ psi$$

$$f_{c_2}^{1+} = -514 + 912 = +398 \ psi$$

(Equation 16)

If the tensile strength of concrete is f_t = 420 psi, then column (1) should be expected to crack, i.e., the entire load T_1 would be carried by the steel reinforcement. Under such condtions, a load redistribution would occur, resulting in a large increase in T_2, with susequent cracking of columns (2) as well. The final load distribution will therefore depend on A_{st}^1 and A_{st}^2 only. That is to day, if both columns crack it is irrelevant whether t_1 is small or large. Moreover, A_c^1 and A_c^2 will no longer play any role in the problem. In fact:

$$\alpha^{1+} = \frac{1000}{2 \times 30000} = 0.01667$$

$$\beta^{1+} = \frac{1.155 \times 1000}{4 \times 30000} = 0.00962$$

(Equation 17)

$$T_1^{1+} = \frac{0.00962\ P}{1.5 \times 0.01667 + 0.00962} = 0.278P$$

$$T_2^{1+} = \frac{0.01667 \times 0.866}{1.5 \times 0.01667 + 0.00962} = 0.416P$$

(Equation 18)

It has been shown that if our sample structure is fully cracked, then creep has no influence whatsoever on the final load distribution. It may be hypothesized, however, that the concrete tensile strength in Column (2) is higher, say ft = 1500 psi. The question is then asked, what is now the load distribution. The problem may be solved by computing the total load "C" carried by concrete in Column (1) at time shortly before $t = t_1$, and assuming that, as Column (1) cracks, load will be transferred simultaneously to joint and to the steel of column (1).

Initial Load Distribution with Concrete in Column (1) Fully Cracked

$$\alpha_c = \frac{1000}{2 \times 7.5} \frac{1}{E_c^0} = \frac{66.6}{E_c^0}$$

$$\beta_c = \frac{1.155 \times 1000}{100 + 4 \times 7.5} \frac{8.875}{E_c^{\,0}}$$ (Equation 19)

$$T_1 = \frac{8.875}{1.5 \times 66.6 + 8.875} P = 0.082\ P$$

$$T_2 = \frac{0866 \times 66.6}{1.5 \times 66.6 + 8.875} P = 0.531\ P$$ (Equation 20)

$$T_1 = 0.385\ P_0 + 0.082\ (P_1 + C) - C$$

$$T_2 = 0.355\ P_0 + 0.531\ (P_1 + C)$$ (Equation 21)

with C = -.598 x 100 = -59.8 kips we get:

$$\left.\begin{aligned} T_1 &= +2.6\ kips \\ T_2 &= +56.9\ kips \end{aligned}\right\} \quad t_1 \rightarrow \infty$$ (Equation 22)

If t_1 is sufficiently small, it may be assumed that P_0 and P_1 are applied simultaneously at t = 0, in which case:

$$\left.\begin{aligned} T_1 &= 0.082 \times 100 = +8.2\ kips \\ T_2 &= 0.531 \times 100 = +53.1\ kips \end{aligned}\right\} \quad t_1 = 0$$ (Equation 23)

The difference between (22) and (23) is not large. Note that superimposing the load distribution after creep due to P_0 (equation 13) with the load distribution corresponding to the cracked structure under P_1 leads to:

$$T_1 = -0.385 \times 200 + 0.082 \times 300 = -42.4\ kips$$

$$T_2 = -0.355 \times 200 + 0.531 \times 300 = 88.3\ kips$$ (Equation 24)

which are entirely unrealistic figures. Note also that an "exact" stress analysis for the case when t_1 is large (equations (19) and (20)) would not be feasible for moderately complex structures.

APPENDIX B TO APPENDIX 3B

EARTHQUAKE ANALYSIS

3B.B EARTHQUAKE ANALYSIS

The computation of seismic stresses was carried out on the basis of the fundamental mode of the containment structure associated with maximum response. The peak of the response curve (=0.47g) for 2 percent critical damping and 0.2g peak ground acceleration was used to determine:

1. The stress-resultant N_ϕ at the center of the opening (in the shell without the opening) for the horizontal component of earthquake action oriented in the direction normal to the openings.
2. The in-plane shear stress-resultant at the center of the opening (in the shell without the opening) for the horizontal component of earthquake notion oriented at 90° with the direction normal to the opening.
3. The stress-resultant $N_{\phi\theta}$ at the center of the opening (in the shell without the opening) for the vertical component of motion associated with 0.2g peak ground acceleration.

The influence of the opening on the above seismic loads was evaluated as follows:

a. The stress-resultant and stress-couple distributions and, therefore, the stress-concentration factors corresponding to (1) and (3) were conservatively computed on the basis of the finite-element results for dead load.

b. The stress concentration factors corresponding to (2) were determined on the basis of Lakerkerker's solution[11]. (See Figure 3) for a shell with a hole subjected to torsion, i.e., to a pure membrane shear $N_{\phi\theta}$ at the location of the opening, (in the shell without the opening). Note that the stress concentration factors are slightly larger than those corresponding to the plate solution. In computing stresses at elements away from the edge of the opening, however, the stress concentration factor was assumed to decrease as in the plane solution.

In determining the values shown in Table 4-3, the absolute value of the contribution of the vertical component of motion (3) was added to the absolute value of the contributions of the two horizontal components [(1) and (2)].

ADDENDUM TO APPENDIX 3B

ADDENDUM TO THE REPORT ON: DESIGN OF LARGE OPENING REINFORCEMENTS FOR CONTAINMENT VESSEL

OCTOBER 16, 1968 ADDENDUM TO GAI REPORT NO. 1683

Robert E. Ginna Nuclear Power Station

J. D. Riera, Ph.D.
D. K. Croneberger
K. E. Nodland

3B.C INTRODUCTION

The analysis and design of reinforcement for the large openings in the containment vessel for the Robert Emmett Ginna Nuclear Plant were described in the Third Supplement to the Final Facility Description and Safety Analysis Report (FSAR). This addendum to the aforementioned report provides supplemental information, including certain construction procedures, and additions or corrections to the basis report. The final design is reflected on the attached revised Drawings D-421-023 (Figure Drawing 2), and D-421-024 (Figure Drawing 1).

1 DESIGN

1.1CONCRETE SHEAR

Splitting planes were hypothesized parallel to the surface of the shell through the various 1ayers of concrete reinforcement and tendon conduit. The in plane shear stresses are produced by the interrupted horizontal reinforcing bars as well as by radial forces produced by elliptical rebar rings and draped tendons. Sufficient steel has now been provided in the form of straight or hooked radial bars and ties to develop the total shear stress across the hypothesized planes. The shear stresses are conservatively assumed to be the summation of the loads resisted by the elliptical bars on the vertical axis due to the factored pressure load. That is to say, the shearing force exerted across a plane through Layer 6 (see attached Drawing No. D-421-024, Figure Drawing 1) is equal to the summation of rebar forces on Layers 6 and 7 on the vertical axis. The maximum shear stress on the dowels due to the aforementioned load does not exceed the yield stress of the dowels. The dowels are anchored by mechanical anchorage (180° or 90° hooks) and/or sufficient bond development length which is determined on the basis of Ultimate Strength Design provisions of ACI 318-63. All rebars provided to resist the aforementioned loads consist of A15 material with a 40 ksi minimum guaranteed yield strength.

1.2INTERACTION DIAGRAMS

For derivation of Equations (5.1) through (5.5) refer to:

a. ACI 318-63 chapters 16 and 19.

b. "Design of Concrete Structures" by 0. Winter et. al., chapter 5.

It should be pointed out that all points on the interaction diagram are computed with respect to shell reference surface as shown in Figures 19 through 23. That is, under compression and bending, "N" and "H" were transferred from the plastic centroid to the shell reference surface. Under tension, "N" was transferred from the center of gravity of the reinforcing steel to the shell reference surface.

1.3EARTHQUAKE DESIGN

The stresses due to earthquake motions, as described in section 4.3.2c on Page 29 and in Appendix B of the report, were determined on the basis of the acceleration response spectra for 0.20g maximum ground acceleration (Figure 5.1.2-8 of the FSAR) and the resultant load diagram in the form of a triangular distribution with the base of the triangle at the top of the structure.

1.4THERMAL GRADIENTS

The thermal gradients described in section 1.2 on Page 2 and Figure 12 of the report are based upon steady stare (operating) conditions.

1.5PENETRATION MATERIAL

As stated in section l.4d on Page 7 of the report the penetration materials (steel plate) conform to ASTM A516 Grade 60 Firebox Quality modified to ASTM A300. The steel plate has a nil ductility transition temperature, as measured by a Charpy V-notch specimen of at least 30° F below the minimum service metal temperature. This requirement on NDTT applied to all penetration materials as well as the liner plate.

1.6WORKING STRENGTH DESIGN

The load combinations listed in section 1.3 on page 3 and in Table 4-1 of the report are based upon an ultimate strength design approach. In addition, the load combinations were considered in a working strength design approach (i.e., load factors equal 1.0) when the stress/strain criteria is established by the ASME Nuclear Vessels Code and Chapter 26 - Prestressed Concrete of ACI 318-63. For the design of the opening reinforcement, the items for which working strength design therefore applied included:

a. Liner plate and penetration barrel.

b. Anchorage of interrupted horizontal bars (concrete bearing stresses).

1.7ANCHORAGE PLATE BEARING STRESS

The concrete bearing stress, as defined by Equation (5.8) on page 58 of the report, shall not exceed the compressive strength of the concrete when the load is applied, which for purposes of this design is assumed to be the 28 day compressive strength. The calculated bearing stress is 3640 psi which is less than the allowable value of 3670 psi determined by Equation (5.8).

It should be noted that the calculated bearing stress is based upon the factored pressure load while the allowable stress is on the basis of a working strength design.

1.8INSULATED LINER TEMPERATURE INCREASE

The change in liner temperature of 2°F, as referred to in section 1.3 on page 4 of the report, represents the mean temperature rise from normal operating conditions to the time associated with the maximum pressure as shown on the transients for the factored pressure (90 psig). Verification of the capability of the insulation to restrict the liner temperature change to this specified value is described in Appendix 5B of the FSAR.

1.9HIGH STRENGTH REBAR

The use of 60 ksi rebars was basically restricted to the immediate vicinity of the stress concentration (i.e., the elliptical bars and the horizontal bars draped around the hole). Specific requirements for 60 ksi material (A432) are shown on attached Drawing No. D-421-023 (Figure Drawing 2).

1.10PROOF TEST INSTRUMENTATION

Measurements of displacements, strains, and cracking about the opening for the equipment access hatch will be obtained as follows:

a. Displacement Measurements

Horizontal and vertical displacements of the reinforced area around the opening will be obtained with linear variable differential transformers (LVDT) mounted on a structure not affected by the test. On the horizontal axis, on one side only, six horizontal and vertical displacements will be obtained at equally spaced locations extending from a location two feet from the edge of the opening to a location twenty-one feet from the edge of the opening.
On the vertical axis, on the top side only, the quantity and locations of measurements to be obtained will be identical to that described herebefore. On the horizontal axis, on the opposite side previously mentioned, two horizontal and vertical displacements will be obtained at one location two feet from the edge of the opening and another location seven feet from the edge of the opening.

b. Strain Measurements

Horizontal and vertical strains will be measured on the rebar nearest the exterior concrete face at those locations described for displacement measurements.

c. Concrete Crack Measurements

One upper quadrant of the area around the opening extending from the edge of the hale to a line 3 ft - 6 in. outboard of the thickened concrete portion of the shell will be coated and detailed measurements made of spacing and width of cracks.

1.11 OPERATING CONDITIONS

Refer to Table 4-1 on page 35 of the report. The first four load combinations reflecting normal operating conditions are based on an uncracked shell.

The computer output for Element No. 77 resulted in:

N_θ = + 6.5 K/in. for Load Comb. (2)

N_θ = - 15.6 K/in. for Load Comb. (4)

Maximum tensile stresses will be:

σ = 155 psi in the concrete for uncracked concrete, and

σ = 1625 psi in the rebar for cracked concrete.

1.12SHEAR - DIAGONAL TENSION

The ACI 318-63 recognizes the punching shear to be critical at a distance $\frac{"d"}{2}$ out from the periphery for slabs and footings (See Section 1207 and 1707). A beam type of diagonal tension failure is impossible due to the geometry and two directional stresses in the shell. We believe that a punching mode of failure is the type of failure that should be and has been investigated. These shear stresses included in the computer output take into account the effect of the pressure on the door plus the reinforced area.

1.13NORMAL SHEARS

The average normal shears at the edge of the thickened (reinforced) area are:

Top horizontal edge:v = 38 psi

Vertical edge: v = 29 psi

1.14RADIAL SHEAR AT THE PERIPHERY OF THE OPENING

The assumption of a uniform radial shear at the periphery of the opening was made solely for the finite element method of stress analysis. This assumption was judged to be reasonable, as the radial displacements about the periphery of the hole are essentially constant. Furthermore, a variation of the radial shears was made and was found to have little effect on the resulting stress resultants and stress couples. Nevertheless components including the shear ring and reinforcement for diagonal tension were designed for a radial shear twice the computed value based upon a uniform distribution.

1.15ACCIDENT TEMPERATURE EFFECTS

Item 2(b), page 32 of the report, indicates that the concrete around the opening was considered to be uniformly heated to 192°F, to a depth of 0.55 in. This is an approximation, arrived at by using the area under a step gradient equal to the area under the actual gradient remote from the boundaries (i.e., the inside or outside faces of the wall).

1.16ANALYTICAL MODEL FOR DIFFERENT LOAD COMBINATIONS

The coefficients listed for the various load combinations are developed on the basis of the absolute values used in the stress analysis, which were dead load, final prestress (0.60 f_s), test pressure (p = 69 psig), accident temperature based on factored pressure load (T = 312°F), and 0.20g ground acceleration. All load combinations representing operating conditions are based on the uncracked model. All other load combinations are based on the same cracked model. An inspection of the stress resultants and stress couples for various cracked models indicated that this approach is valid, in that changes in the cracking pattern did not significantly alter the stress resultants and stress couples.

1.17SHEAR REINFORCEMENT

$$v_u = \phi\left(A_{sv}f_y + A_{sd}\frac{f_y - f_r}{2}\right)$$ (Equation 5.7)

The first term within the bracket is the "stirrup" effect to resist diagonal tension. The cross-sectional area of "A_{sv}" must be properly anchored in order to be considered effective. In the actual design the effect of the first term ii found to be negligible.

The second term is intended to represent the dowel action of reinforcing steel intersecting a potential crack. Tests on studs [a] have indicated that the ultimate shear capacity is equal to the

a. Nelson Stud Welding Manual No. 21, August 1, 1961, Gregory Industries, Inc.

ultimate tensile capacity of the steel. Further tests on rebar and discussion of the shear-friction hypothesis[a] indicate that the steel normal to a crack will act in tension and that for shear across a rough concrete to concrete interface:

$$A_{sd} = \frac{v_u}{1.4 f_y}$$

Therefore, the second term in equation (5.7) is only 35 percent of the value predicted by the shear friction hypothesis. This conservatism was employed to minimize the amount of ship-page required to develop the capacity at the hypothesized crack.

The out-of-plane shear stresses in the meridional direction and in the hoop direction t_ϕ were combined as a resultant shear stress acting in the plane of the shell. That is:

$$\tau_{in\ plane} = (\tau_\phi^2 + \tau_\theta^2)^{1/2}$$

Tee's and straight bars were provided to carry this shear by steel alone, that is, assuming the concrete to be cracked. It should be noted that the concrete stress, so computed, $\tau_{in\ plane}$ is less than $\sqrt{c} = 4\phi\sqrt{f_c'}$.

The meridional shear along the vertical axis can be resisted by unreinforced concrete. However, sufficient reinforcement has been provided to carry this shear by steel alone.

The hoop shear along the horizontal axis has been investigated and sufficient reinforcement provided to carry this shear by steel alone.

1.18EQUATION (5.11)

Equation (5.11) on page 60 should be as follows:

$$f_{si} = \frac{t_x i}{A_s}$$

1.19REBAR LOCATED AWAY FROM THE BARREL

The average clearance between elliptical steel and barrel is only 11 in. or about 17 percent of the shell thickness. The elliptical reinforcing steel arrangement around the access barrel will:

---

a. R. F. Mast: "auxiliary Reinforcement in Concrete Connections," Journal ASCE, Vol. 94, No. ST6, June 1968, pp. 1485-1504.

a. Punish enough reinforcing steel close to the barrel on the top (Element No. 77) to resist the high hoop tension wider pressure load, and

b. Provide enough space between the barrel and the first ring for anchorage of the terminated hoop steel.

The maximum distance from the barrel to the first elliptical ring is at the horizontal axis, 18 in. The stresses at this point (Element No. 101) are all compressive. See interaction diagram Figure 21 of the report.

For stresses on the top (Element No. 77), see Figure 22 of the report. For stresses on the 45 degree axis from the horizontal (Element 73 and 74), see Figure 19 of the report.

1.20VERIFICATION OF ANALYSIS

Hansen, Holley and Biggs (H.H.&B.) as consultants to Rochester Gas & Electric Corporation did make limited independent checks on the GAl analysis described in the report. The scope of the H.H.&B. analysis was as follows, with all models based upon uncracked plain concrete:

a. Using two separate programs, H.H.&B. analyzed the GAl test problem (refer to Section 4.1 of the report); Prato's program [reference 16 of the report, (Mixed Finite Element Method)] and Rodriguez's program (Displacement Method) gave results in good agreement with each other and with the other results included in the report.

b. Prato's program was thereafter used for the solution of the following canes based upon the actual containment cylinder and opening radii and a Poisson's ratio of 0.15:

   1. An internal pressure of 90 psig with loading on the perimeter of the opening limited to the component along the opening axis (i.e., no component normal to the opening was considered). The shell was considered to be of constant thickness (42 in.), with a modulus of elasticity of 4.0×10^6 psi.
   2. Same as (1) except that the shell was thickened to 66 in. in the vicinity of the opening within a boundary which varied from 119 in. to 144 in. from the edge of the opening chosen to follow the boundary of selected elements.
   3. Same as (1) above except that the constant thickness was reduced to 4.2 in. and the modulus of elasticity was increased to 40×10^6 psi. These changes were intended to indicate the sensitivity of the analysis to a greatly reduced bending stiffness with no change in the membrane stiffness.
   4. Same as (1) above, except that internal pressure is not considered and the loading parallel to the axis of the opening was defined as "pr/4 cos 2θ" where "p" equals 90 psig and "r" equals the opening radius of 85.7 in.
   5. Same as (4) above, except that the loading parallel to the axis of the opening was defined as "pr/4 sin 2θ

Stress resultants "N_θ" along the horizontal and vertical axes of symmetry are compared on the attached Figure I with similar results obtained by the GAl analysis. This comparison is based on the models described in (1) and (2) above. The correlation is excellent.

Even in the extreme case investigated to determine sensitivity to reduced bending stiffness (Case No. 3), sufficient rebar is available without yielding to resist the calculated stress resultants (N_θ) due to the pressure load commencing at a distance 10 in. from the edge of the opening. Sufficient rebar is available even considering the high stress resultant at the edge of the opening if the stress resultants are integrated for a distance approximately 24 inches from the opening edge. Cases Nos. 4 and 5 were reported to indicate that the solution is not sensitive to variations in the radial load distribution at the edge of the opening.

1.21TEST PROBLEM

On page 21 of the report, the coefficient "ν" for the test problem is 0.62 instead of 1.17. The coefficient "ν" for the R. E. Ginna Containment Vessel is $\mu = 0.34$ (equipment hatch, based on typical thickness). The conclusion is still valid.

1.22ACCIDENT TEMPERATURE

Refer to Item 2 on page 32 of the report. Further verification of the numerical results given in the report revealed that the equivalent pressure applied by the barrel (penetration sleeve) on the concrete is 320 instead of 160 psi, when the barrel is heated due to accident temperature. This error affects the stress-resultants and stress-couples for loading condition No. 4 (accident temperature). Therefore, the values indicated in Table 4-3, page 43, should be replaced by those given in the attached Table I. It can readily be seen that at the most critical location, i.e., in element No. 77 and in the hoop direction, the difference is:

$\Delta N_\theta =$ 14.09 - 7.93 = 6.56 K/in.

$\Delta M_\theta =$ 149.08 - 68.66 = 70.42 Kips-in./in.

Inspection of the interaction diagram for element No. 77, Figure 22 of the report shows that displacing the points closer to the edge of the diagram by the amounts computed above, still leaves them well inside the interaction diagram. The proposed design is therefore not affected by the computational error referred to above.

Note, that even if the stress-resultants and stress-couples due to accident temperatures given in the attached Table were doubled, the resulting stress-resultants and stress-couples for all load combinations would still fail within the interaction diagrams.

2 CONSTRUCTION

2.1CONSTRUCTION SCHEDULE

The schedule for placement of concrete is shown on the attached Drawing SS-400-659 (Figure Drawing 3). This drawing also reflects the location of construction joints.

2.2CONCRETE REMOVAL

a. Condition of Old Concrete

Prior to placing concrete which will abut a joint produced by concrete removal, the joint will be thoroughly cleaned with filtered air and water spray to remove all loose material, and an inspection will be made for cracks. Any visible cracks will be removed using hand tools, and patched if necessary. Special attention will be given to detect possible cracks oriented parallel to reinforcing bars which might produce a "splitting type" bond failure when the structure is loaded. The reinforcing bars that were exposed by the concrete removal operation have been or will be thoroughly cleaned to remove bonded concrete or mortar to ensure the bond is achieved with the new concrete. It should be pointed out that the air hammers employed could only remove small particles of concrete and it was impossible to produce significant cracking to ease the operation.

b. Construction Joint Preparation

Horizontal and vertical construction joints were, or are, to be prepared for receiving the next pour by either sandblasting, air/water jet, bush hammering, or other means to remove all coatings, stains, debris, or other foreign material.

On construction joint surfaces in the Containment Vessel, including all vertical joints in the cylindrical shell and all joints in the dome, an epoxy resin (Colma Bonding Compound as manufactured by Sika Chemical Corporation) was, or is, being used. This applies to the vertical joints in the vicinity of the large openings.

The horizontal joints will be dampened (but not saturated), and then thoroughly covered with a coat of neat cement mortar of similar proportions to the mortar in the concrete.

The mortar will be approximately 1/2 inch thick and fresh concrete will be placed before the mortar has attained its initial set.

2.3CONCRETE WORK

a. Pour Limits

Construction joints will be located as shown on the attached Drawing SS-400-659 (Figure Drawing 3). A review was made of the shear stresses at construction joints and it was found that sufficient rebars exist to resist the shears without contribution from the concrete. The maximum concrete lift height is 10 ft - 0 in. and maximum concrete quantity per pour is approximately 63 cubic yards.

b. Concrete Mix and Curing

The basic concrete mix was initially developed to minimize shrinkage. This involved selection of a course aggregate (dolomite) and careful selection of additives (water reducer/ retarder). Special attention has been given to orientation of construction joints to permit adequate venting, thereby making possible a sound interface between new and old concrete. Initial and final concrete curing will be the wet method as specified in ACI 301-66.

2.4RETENSIONING TENDONS

Relaxation losses which account for approximately two-thirds of the total losses in a tendon were estimated, based on "A Study of Stress Relaxation in Prestressing Reinforcement," by D. D. Mogura et. al., PCI Journal, April 1964. In order to provide the required prestress force at the base of the structure at the end of plant life (40 years), it will be necessary to retension those tendons which are draped around the openings for the equipment hatch and the personnel lack and therefore experience higher than typical friction losses. According to the foregoing procedure the minimum time delay for retensioning to ensure required prestress at the base of the cylinder at the end of plant life is 1,000 hours.

The total increase in prestress force at the top of the cylinder due to retensioning the tendons at the equipment access hatch is approximately 750 kips. This force produces negligible changes in concrete stress at the opening.

2.5REBAR SPLICES

The normal procedure for locating bar-to-bar splices in the containment structure was to have no more than one-third of the splices in one plane with the minimum dimension between planes being 3 ft - 0 in. In the vicinity of the opening the splices are staggered to the maximum extent practical with no more than one half of the splices in one plane. The distance between two planes approximating the location of splices will be 20 to 24 inches. Splices on bars in one layer and in bars from layer to layer are staggered to the maximum extent permitted by existing conditions. The minimum spacing between splices on one bar will be 8 ft - o in., except for limited locations which consist primarily of locations where in-place splices were, or will be, removed for mechanical testing, and of locations on the inner band of horizontal bars where limited access precluded splice removal.

2.6TENDON CONDUIT

The tendon conduit, including that in the vicinity of the large openings, consists of six inch nominal diameter Schedule 40 pipe conforming to ASTM A53. The splices on this conduit consist of either standard threaded or welded couplings. The former were used only in the form of a half coupling connecting the tendon coupling enclosure to the conduit.

Table I
STRESS AROUND EQUIPMENT HATCH LOADING CONDITION NO. 4 - Accident Temperature

STRESS AROUND EQUIPMENT HATCH
LOADING CONDITION NO. 4
Accident Temperature

Element	Axial Direction		Hoop Direction		Membrane Shear	Normal	Shears
	N_ϕ	M_ϕ	N_θ	M_θ	$N_{\phi\theta}$	Q_ϕ	Q_θ
11	- 3.46	16.08	0.93	3.07	-0.14	-0.14	-0.02
22	- 4.18	18.08	1.36	4.78	-0.15	-0.04	0.02
33	- 5.00	17.38	4.31	43.32	-0.35	-0.27	-0.26
44	- 6.57	21.37	5.90	60.11	-0.71	-0.93	-0.40
55	- 8.19	26.80	8.15	82.63	-1.09	-1.12	-0.96
66	-10.11	43.34	10.63	108.75	-1.85	-1.28	-0.54
77	-12.54	48.87	14.49	149.08	-2.47	2.59	1.85
25	- 0.30	6.68	- 0.18	2.78	-1.16	-0.23	-0.10
49	0.04	16.41	- 0.30	5.03	-2.97	-0.10	-0.17
73	2.29	26.74	- 3.14	-15.27	-6.04	2.15	0.08
74	- 0.19	66.77	- 2.35	-47.19	-9.40	-4.19	-0.88
94	0.66	1.19	- 1.86	- 4.47	-0.07	-0.01	-0.32
97	3.36	19.21	- 3.48	7.58	-0.37	-0.09	0.42
99	5.75	- 30.87	- 5.48	10.01	-0.70	0.39	1.66
100	9.42	- 91.38	- 7.65	3.14	-1.85	1.47	4.05
101	10.95	-208.35	-10.68	-20.82	-4.48	-3.04	8.35

Note: N_ϕ, N_θ, $N_{\phi\theta}$, Q_ϕ and Q_θ in Kips/in. M_ϕ, and M_θ in Kips.

Values computed by finite-element analysis of cracked shell.